

1 **Molecular and seasonal characteristics of organic vapors in**  
2 **urban Beijing: insights from Vocus-PTR measurements**

3

4 Zhaojin An<sup>1,2</sup>, Rujing Yin<sup>3</sup>, Xinyan Zhao<sup>1</sup>, Xiaoxiao Li<sup>4</sup>, Yuyang Li<sup>1</sup>, Yi Yuan<sup>1</sup>,  
5 Junchen Guo<sup>1</sup>, Yiqi Zhao<sup>1</sup>, Xue Li<sup>5</sup>, Dandan Li<sup>1</sup>, Yaowei Li<sup>2</sup>, Dongbin Wang<sup>1</sup>,  
6 Chao Yan<sup>6</sup>, Kebin He<sup>1</sup>, Douglas R. Worsnop<sup>7,8</sup>, Frank N. Keutsch<sup>2</sup>, Jingkun  
7 Jiang<sup>1,\*</sup>

8

9 <sup>1</sup>State Key Joint Laboratory of Environment Simulation and Pollution Control,  
10 School of Environment, Tsinghua University, 100084, Beijing, China

11 <sup>2</sup>School of Engineering and Applied Sciences, Harvard University, Cambridge,  
12 Massachusetts 02138, USA

13 <sup>3</sup>Key Laboratory of Industrial Ecology and Environmental Engineering (Ministry  
14 of Education), School of Environmental Science and Technology, Dalian  
15 University of Technology, 116024, Dalian, China

16 <sup>4</sup>School of Resource and Environmental Sciences, Wuhan University, 430072,  
17 Wuhan, China

18 <sup>5</sup>School of Environment, Henan Normal University, 453007, Xinxiang, China

19 <sup>6</sup>Joint International Research Laboratory of Atmospheric and Earth System  
20 Research, School of Atmospheric Sciences, Nanjing University, 210023,  
21 Nanjing, China

22 <sup>7</sup>Institute for Atmospheric and earth System Research / Physics, Faculty of  
23 Science, University of Helsinki, Helsinki 00014, Finland

24 <sup>8</sup>Aerodyne Research, Inc., Billerica, Massachusetts 01821, USA

25 \*Corresponding author: Jingkun Jiang (email: [jiangjk@tsinghua.edu.cn](mailto:jiangjk@tsinghua.edu.cn))

26

27

## 28 **Abstract**

29 Understanding the composition and evolution of atmospheric organic vapors is  
30 crucial for exploring their impact on air quality. However, the molecular and  
31 seasonal characteristics of organic vapors in urban areas, with complex  
32 anthropogenic emissions and high variability, remain inadequately understood.  
33 In this study, we conducted measurements in urban Beijing during 2021-2022  
34 covering four seasons using an improved Proton Transfer Reaction-Mass  
35 Spectrometer (Vocus-PTR MS). During the measurement period, a total of 895  
36 peaks were observed, and 512 of them can be assigned to formulas. The  
37 contribution of  $C_xH_yO_z$  species is most significant, which composes up to 54%  
38 of the number and 74% of the mixing ratio of total organics. With enhanced  
39 sensitivity and mass resolution, various species with sub-ppt level or multiple  
40 oxygens ( $\geq 3$ ) were observed, with 44% of the number measured at sub-ppt  
41 level and 38% of the number containing 3-8 oxygens. Organic vapors with  
42 multiple oxygens mainly consist of intermediate/semi-volatile compounds, and  
43 many formulae detected were reported to be the oxidation products of various  
44 volatile organic precursors. In summer, the fast photooxidation process  
45 generated organic vapors with multiple oxygens and lead to an increase in both  
46 their mixing ratio and proportion. While in other seasons, the variations of  
47 organic vapors with multiple oxygens were closely correlated with those of  
48 organic vapors with 1-2 oxygens, which could be substantially influenced by  
49 primary emissions. Organic vapors with low oxygen content ( $\leq 2$  oxygens) are  
50 comparable to the results obtained by traditional PTR-MS measurements in  
51 both urban Beijing and neighboring regions.  
52

## 53 1 Introduction

54 Volatile organic compounds (VOCs) play a crucial role in the formation of ozone  
55 and fine particulate matter (PM<sub>2.5</sub>) in the atmosphere, subsequently affecting air  
56 quality, climate, and human health (Carter, 1994; Williams and Kopppmann,  
57 2007; Jimenez et al., 2009; Hallquist et al., 2009). The sources and atmospheric  
58 evolution of VOCs in the atmosphere are complex due to the coexistence of  
59 compounds from primary emissions as well as secondary formation (Gentner  
60 et al., 2013; Gilman et al., 2015; Millet et al., 2015). Understanding their  
61 molecular characteristics is essential for studying their hydroxyl radical (OH)  
62 reactivities, ozone and secondary organic aerosol (SOA) formation potentials.  
63 However, the diverse range of species and wide distribution of oxidation  
64 products of atmospheric VOCs make it challenging to unravel their molecular  
65 properties (Goldstein and Galbally, 2007).

66 Instrumental advances have allowed for improving the understanding of the  
67 compositions and variations of VOCs at the molecular level, especially for  
68 oxygenated VOCs (OVOCs). Gas chromatography or multidimensional gas  
69 chromatography coupled with mass spectrometry is the most commonly used  
70 technology for VOC measurement, capable of detecting major non-methane  
71 hydrocarbons and select OVOCs (Lewis et al., 2000; Xu et al., 2003; Noziere  
72 et al., 2015). Proton Transfer Reaction-Mass Spectrometry (PTR-MS) enables  
73 real-time detection of VOCs without pre-concentration and separation, greatly  
74 enriching the molecular understanding of OVOCs due to its high sensitivity to  
75 oxygen-containing compounds (Hansel et al., 1995; De Gouw and Warneke,  
76 2007; Yuan et al., 2017). Hundreds of OVOCs have been detected and  
77 characterized in different areas using PTR-MS, e.g. urban (Wu et al., 2020),  
78 suburban (He et al., 2022), and forest areas (Pugliese et al., 2023). Recent  
79 developments in the ion-molecule reactor (IMR) configuration have greatly  
80 increased sensitivities and concurrently lowered the limits of detection of PTR-  
81 MS by several orders of magnitude by incorporating radio frequency electric  
82 fields to focus ions (Breitenlechner et al., 2017; Krechmer et al., 2018; Reinecke  
83 et al., 2023). A consequential issue is that these advanced PTR-MS typically  
84 need to eliminate lighter ions to protect the detector from overload, and similar  
85 to traditional PTR-MS, they are incapable of obtaining molecular structure  
86 information.

87 These improvements have expanded the detection capabilities of PTR-MS,  
88 particularly for organic vapors with lower volatility and multiple oxygens ( $\geq 3$ )  
89 (Riva et al., 2019), which enables the simultaneous measurement of VOC  
90 precursors and their primary, secondary, and higher-level oxidation products  
91 using a single instrument (Li et al., 2020). Despite their low concentrations,  
92 these vapors may condense on pre-existing aerosols and make a significant  
93 contribution to secondary aerosol growth and cloud condensation nuclei

94 (Bianchi et al., 2019; Pospisilova et al., 2020; Nie et al., 2022). Organic vapors  
95 with multiple oxygens are likely to be simultaneously detected by other chemical  
96 ionization mass spectrometry (CIMS), e.g., nitrate ( $\text{NO}_3^-$ ), iodide ( $\text{I}^-$ ), bromide  
97 ( $\text{Br}^-$ ), and ammonium ( $\text{NH}_4^+$ ) (Riva et al., 2019; Huang et al., 2021), which are  
98 widely used for measuring oxygenated organic compounds in the atmosphere  
99 (Bianchi et al., 2019; Ye et al., 2021; Huang et al., 2021). Therefore, using these  
100 improved PTR-MS can supplement our understanding of oxygenated organic  
101 vapors and facilitate the study of atmospheric chemical evolution of organics  
102 (Wang et al., 2020a).

103 The improved PTR-MS systems have gradually gained traction in research  
104 applications over the past few years, including measuring organics in controlled  
105 lab studies (Zaytsev et al., 2019a; Zaytsev et al., 2019b; Riva et al., 2019; Li et  
106 al., 2022a; Li et al., 2024a), emission sources (Sreeram et al., 2022; Yu et al.,  
107 2022; Yacovitch et al., 2023; Wohl et al., 2023; Jahn et al., 2023), and ambient  
108 air. For ambient measurements, observations in forested regions have been  
109 extensively conducted to study the compositions, variations, fluxes, and  
110 emissions of organics from different plants (Li et al., 2020; Li et al., 2021; Huang  
111 et al., 2021; Fischer et al., 2021; Thomas et al., 2022; Vettikkat et al., 2023;  
112 Vermeuel et al., 2023). Terpenes and their oxidation products with oxygen  
113 number up to 6 have been detected (Li et al., 2020). Diterpenes have been  
114 directly observed in the ambient air for the first time owing to the substantial  
115 improvement in sensitivity of Vocus-PTR (Li et al., 2020). Ambient  
116 measurement has been also conducted on a mountain in China, which found  
117 that terpenes and their oxidation products dominate the detected organic  
118 compounds, while the influence of industrial emissions can also be observed  
119 (Zhang et al., 2024).

120 In urban atmospheres, the sources and evolution of VOCs are considerably  
121 complex, potentially exhibiting distinct characteristics compared to forested  
122 areas. Several studies have carried out measurements in urban air using these  
123 improved PTR-MS. Jensen et al. (2023) conducted a one-month observation to  
124 address the production of reliable measurements. Coggon et al. (2024)  
125 evaluated the fragmentation and interferences of a series of urban VOCs.  
126 Pfannerstill et al. (2023 and 2024) measured hundreds of VOCs to calculate  
127 their emission fluxes in Los Angeles. A few low-signal species including  
128 dimethylamine, icosanal, dimethyl disulfide, and siloxanes emitted from diverse  
129 emission sources have been detected as a result of the enhanced sensitivity  
130 (Wang et al., 2020b; Chang et al., 2022; Jensen et al., 2023). However, the  
131 understanding of organic vapors with multiple oxygens in urban air, including  
132 their species, mixing ratios, diurnal profiles, and seasonal variations, remains  
133 inadequate.

134 In this study, we conducted measurements of organic vapors using a Vocus-  
135 PTR in urban Beijing during 2021-2022, covering four seasons. We present

136 general characteristics of measured organic vapors and compare them with  
137 traditional PTR-MS and previous Vocus-PTR measurements. We focus on  
138 organic vapors with multiple oxygens (three or more), which have rarely been  
139 individually analyzed in previous studies due to their low mixing ratios. Their  
140 chemical compositions, atmospheric mixing ratios, diurnal and seasonal  
141 variations are reported. Cluster analysis is further conducted to resolve the  
142 main driving factors of their variations.

## 143 **2 Methods**

### 144 **2.1 Measurements**

145 The observation site is located in the central area of Tsinghua University, Beijing  
146 (40°0'N, 116°20'E). It is an urban site with no significant direct influence from  
147 industrial activities or heavy-traffic arteries ([Fig. S1](#) in the supporting information,  
148 SI). Details of this site can be found in the previous study (Cai and Jiang, 2017).  
149 Organic vapors were measured by a Vocus-2R PTR-TOF-MS (Tofwerk AG and  
150 Aerodyne Research Inc., referred to as Vocus-PTR hereinafter), which is  
151 situated on top of a fourth-floor tower building, with its sampling inlet positioned  
152 approximately 20 meters above the ground. The observation period is from May  
153 1<sup>st</sup>, 2021 to March 10<sup>th</sup>, 2022, covering four seasons. Detailed information about  
154 observation periods and their corresponding seasons is shown in [Table S1](#).

155 The operating parameters of the Vocus-PTR used in this study are briefly  
156 described here. In PTR-MS, VOCs are ionized via proton transfer by hydronium  
157 ions ( $\text{H}_3\text{O}^+$ ) in the IMR (Hansel et al., 1995; Yuan et al., 2016). The sensitivity  
158 can be quantified based on the proton transfer reaction rate while  
159 simultaneously considering ion transmission, detector efficiency, etc. (Cappellin  
160 et al., 2012; Jensen et al., 2023). The ion source was supplied with a water  
161 vapor flow of 20 sccm. The IMR was operated at 100°C and 2 mbar with axial  
162 voltage of 600 V and quadrupole amplitude voltage of 450 V. The IMR operating  
163 parameters were optimized to minimize the formation of water clusters. Mass  
164 spectra were collected from  $m/z$  11 to  $m/z$  398 with a time resolution of 5 s,  
165 achieving a mass resolution  $\sim 10,000$  for  $\text{C}_7\text{H}_9^+$  throughout the measurement  
166 period. Ambient air was sampled via a tetrafluoroethylene (PTFE) tube (1.35 m  
167 long, 1/4-inch OD) at a flow rate of 3 LPM to reduce wall losses, with only 150  
168 sccm flow entering the Vocus-PTR. The sampling tube was heated to  $50 \pm 5^\circ\text{C}$   
169 during the measurement. A regularly replaced Teflon filter (every 7 days) was  
170 used in front of the sampling line to prevent the orifice from clogging. The data  
171 within 30 minutes after membrane replacement was excluded. Measurements  
172 were made on a 2-hour cycle with 110 min for ambient air, 5 min for zero gas,  
173 and 5 min for fast calibration. The fast calibrations involved the use of mixed  
174 calibration gases, with detailed information available in [Table S2](#).

175 The ambient PM<sub>2.5</sub>, NO<sub>2</sub>, and O<sub>3</sub> data are from a state-operated air quality  
176 station (Wanliu station), located approximately 3.6 km away from our  
177 observation site. The meteorological parameters, including temperature (T),  
178 relative humidity (RH), wind speed, and wind direction are also from Wanliu  
179 station. The diurnal variations of PM<sub>2.5</sub>, O<sub>3</sub>, NO<sub>x</sub>, RH, and T in four seasons are  
180 shown in [Figure S2](#).

## 181 **2.2 Data processing**

182 Data analysis of Vocus-PTR mass spectra, including mass calibration, baseline  
183 subtraction, and high-resolution peak fitting was conducted using Tofware  
184 (v3.2.3, Tofwerk AG and Aerodyne Research Inc.) within the Igor Pro 8 platform  
185 (WaveMetrics, OR, USA). The ambient mass spectra were averaged over 1 min  
186 for subsequent processing in Tofware. The peaklist used for high-resolution  
187 peak fitting was manually made based on mass spectra of both clean days  
188 (PM<sub>2.5</sub> < 75 µg/m<sup>3</sup>) and polluted days (PM<sub>2.5</sub> ≥ 75 µg/m<sup>3</sup>). The maximum mass  
189 error allowed for identifying peaks is 5-10 ppm, which is consistent of the error  
190 of mass calibration. When there are multiple options of formulas meeting the  
191 error limit under, especially at high molecular weights, a peak with oxygen  
192 numbers ≤ 8 and carbon numbers ≤ 20, and lower degree of unsaturation were  
193 selected; otherwise, the peak would be classified as unknown peak. The  
194 maximum peak area residual for each unit mass resolution is 5%. Subsequent  
195 analysis was performed in MATLAB R2022a (The MathWorks Inc., USA).

196 In PTR-MS, the sensitivities of organic vapors are typically determined through  
197 their direct linear correlation with their PTR rate constant ( $k_{\text{PTR}}$ ). Vocus-PTR  
198 utilizes a big segmented quadrupole with a high-pass band filter, which detects  
199 ions < 35 m/z with reduced transmission efficiency (Krechmer et al., 2018).  
200 Consequently, determining sensitivities in Vocus-PTR involves consideration of  
201 both reaction efficiency and transmission efficiency. [Figure S3a](#) shows the  
202 measured sensitivities of mixed calibration gases and their corresponding  $k_{\text{PTR}}$   
203 values. The linear regression between  $k_{\text{PTR}}$  and sensitivities was obtained  
204 based on sensitivities of C<sub>7</sub>H<sub>9</sub><sup>+</sup>, C<sub>8</sub>H<sub>11</sub><sup>+</sup>, C<sub>9</sub>H<sub>13</sub><sup>+</sup>, C<sub>10</sub>H<sub>9</sub><sup>+</sup>, and C<sub>5</sub>H<sub>9</sub>O<sub>2</sub><sup>+</sup> with an R<sup>2</sup>  
205 of 0.87. Sensitivities of other ions in mixed calibration gases may be influenced  
206 by transmission (ions labeled as gray) and fragmentation (C<sub>5</sub>H<sub>9</sub><sup>+</sup>, C<sub>10</sub>H<sub>17</sub><sup>+</sup> and  
207 C<sub>11</sub>H<sub>11</sub><sup>+</sup>). The transmission efficiency of mixed calibration gases was calculated  
208 using sensitivities of mixed calibration gases, as shown in [Figure S3b](#). The  
209 transmission efficiency of mixed calibration gases aligns well with the fitted  
210 transmission efficiency curve, except for C<sub>5</sub>H<sub>9</sub><sup>+</sup>, C<sub>10</sub>H<sub>17</sub><sup>+</sup> and C<sub>11</sub>H<sub>11</sub><sup>+</sup>, which  
211 potentially experience fragmentation (fragmentation of measured ions are  
212 discussed below). For organic vapors without standards, their theoretical  $k_{\text{PTR}}$   
213 were used to constrain sensitivities, while for organic vapors with no theoretical  
214  $k_{\text{PTR}}$ , an average  $k_{\text{PTR}}$  of known species,  $2.5 \times 10^{-9} \text{ cm}^3 \text{ molecule}^{-1} \text{ s}^{-1}$  was used  
215 to constrain their sensitivities. The theoretical  $k_{\text{PTR}}$  of organic vapors are from

216 previous studies (Zhao and Zhang, 2004; Cappellin et al., 2012; Sekimoto et  
217 al., 2017). Average limits of detection (LODs, 1 min) of the measured  
218 compounds were determined using zero-gas background measurements taken  
219 every 2 hours during the observation periods, as shown in [Figure S4](#). The LODs  
220 were calculated as 3 times the standard deviation of the zero-gas background  
221 divided by the obtained sensitivity. The LODs show a correlation with masses;  
222 as masses increase, instrument backgrounds decrease, leading to lower LODs.  
223 This trend was observed for species with different oxygen content, with LODs  
224 around  $0.03 \pm 0.03$  pptv at  $m/z$  200. Note that LODs in this study are one-minute  
225 averages, with raw 1-second data averaged to 1 minute before ToFware  
226 analysis as mentioned before, which may account for the lower LODs  
227 compared to those in Jensen et al. (2023).

228 The fragmentation, water cluster, and interferences for calibrated and  
229 uncalibrated species were corrected. The ratio of the electric field strength (E)  
230 to the buffer gas number density (N) used in our study was 146.9 Td, and the  
231 gradient between BSQ skimmer 1 and skimmer 2 was 9.8 V, which in case  
232 limited the formation of water clusters, promoted the simple reaction kinetics,  
233 and improved the sensitivity, but may lead to stronger fragmentation. For  $\alpha$ -  
234 pinene, we identified its fragments based on GC chromatograms. The Vocus-  
235 PTR was calibrated in GC mode before atmospheric measurement. A total of 4  
236 species were tested in GC mode, including severely fragmented  $\alpha$ -pinene. The  
237 spectrum of  $\alpha$ -pinene showed that the main fragment was  $C_6H_9^+$ . Several long-  
238 chain aldehydes and cycloalkanes may fragment on  $C_5H_8H^+$ , the ion typically  
239 attributed to isoprene in PTR-MS (Gueneron et al., 2015; Pfannerstill et al.,  
240 2023a; Coggon et al., 2024). We corrected isoprene signals following an  
241 approach by Coggon et al. (2024). The correction was calculated as follows:

$$242 \quad m/z \ 69.07_{\text{Corrected}} = S_{69.07} - S_{111.12+125.13} \cdot f_{69.07/(111.12+125.13)} \quad (1)$$

243  $S_{69.07}$  is the signal measured at  $C_5H_9^+$ .  $S_{111.12+125.13}$  is the signal of the isoprene  
244 interferences, referring to  $C_8H_{15}^+$  ( $m/z$  111.12) and  $C_9H_{17}^+$  ( $m/z$  125.13), which  
245 are dehydrated products from octanal and nonanal, respectively.  
246  $f_{69.07/(111.12+125.13)}$  was determined from nighttime data (0:00-4:00) of each period.  
247 Similarly, acetaldehyde was corrected for ethanol fragments. We also checked  
248 the fragments and water cluster list in Pfannerstill et al. (2023a) and Jensen et  
249 al. (2023). When the Pearson correlation coefficient  $r$  is greater than 0.95, the  
250 ions were considered as fragments or water clusters of the parent ion. We also  
251 tried to exclude the effects of unknown fragments and water clusters based on  
252 correlations of times series. Similar to Pfannerstill et al. (2023a), any ion  
253 showing a correlation with another ion with  $r^2 > 0.97$  (if chemical reasonable)  
254 was analyzed for possible water clustering or fragmentation effects and added  
255 up with its parent ion. The ions corrected are specified in [Table S3](#).

256 Here, we discuss the uncertainties of quantification for calibrated and

257 uncalibrated compounds. The uncertainty of calibrated ions ranges from 2% to  
258 16% determined from the standard deviations of the fast calibrations during the  
259 measurement periods. The quantification was conducted for uncalibrated  
260 compounds with their sensitivities constrained by  $k_{PTR}$  linear relationship and  
261 transmission efficiency. The uncertainty of these uncalibrated compounds  
262 arising from linear fitting and transmission efficiency fitting is 20% using Monte  
263 Carlo simulation. Additionally, undetermined fragmentations and water clusters  
264 also contribute to the uncertainty, though we identified some potential  
265 fragments and water clusters through the strength of correlations as previously  
266 indicated. We acknowledge that this method cannot identify all fragments and  
267 clusters, and fragments and clusters may still be present in the measured VOCs  
268 and OVOCs. Further research is needed to explore the impact of fragments  
269 and clusters on the measurements, particularly concerning OVOCs with  
270 multiple oxygens.

271 Double bond equivalent (DBE), carbon oxidation state ( $\overline{OS}_C$ ), and volatility of  
272 organic vapors were calculated to address the chemical and physical properties  
273 of detected organic vapors (see Text S1). The condensational growth rates  
274 contributed by detected organic vapors were simulated using a kinetic  
275 partitioning method, as detailed in Li et al. (2024b). For comparison, the  
276 condensational growth rates of low volatile and extremely low volatile organic  
277 compounds measured by nitrate-CIMS were also simulated (Li et al., 2024b).  
278 The OH reactivities of detected organic vapors were calculated, and the rate  
279 constants are from Data S1 in Pfannerstill et al. (2024) and Table S4 in Wu et  
280 al. (2020). For species with unreported rate constants, we calculated the OH  
281 reactivities for hydrocarbons and OVOCs using the reported median rate  
282 constants of hydrocarbons and OVOCs, respectively.

283 Quantified mixing ratios were further processed by cluster analysis to  
284 investigate their characteristics. Intraclass correlation coefficient (ICC) is a  
285 suitable method for assessing the consistency of trends in unbalanced data. It  
286 quantifies the stability of differences between two sets of measurement results,  
287 enabling evaluation of their consistency. ICC combined with k-means cluster  
288 analysis were used. ICC(C, 1) was selected among several typical consistency  
289 evaluation parameters for its evaluation results exhibit the highest level of  
290 differentiation based on factual evidence (Qiao et al., 2021). ICC(C, 1) was  
291 calculated as follows:

$$292 \quad ICC(C, 1) = (D(X + Y) - D(X - Y)) / (D(X + Y) + D(X - Y)) \quad (1)$$

293 where  $D(\cdot)$  is the arithmetic operators of variance.  $X$  and  $Y$  are two sets of  
294 measurement data, in this case referring to the mixing ratios of any organic  
295 vapors we are concerned about. The ICC matrices of various organic vapors  
296 were subsequently utilized as input for k-means analysis. Square Euclidean  
297 distance was selected to calculate the distances between different organic  
298 vapors.



## 299 3 Results and discussion

### 300 3.1 General characteristics of organic vapors

301 During the measurement period, a total of 895 peaks were observed, and 512  
302 of them can be assigned to formulae, divided into  $C_xH_y$ ,  $C_xH_yO_z$ ,  $C_xH_yN_i$ , and  
303  $C_xH_yO_zN_i$  categories based on their elemental compositions (Fig. 1a).  $C_xH_yO_z$   
304 composes up to 54% of the total number of formulae followed by  $C_xH_yO_zN_i$ ,  
305  $C_xH_y$ , and  $C_xH_yN_i$ , with proportions of 26%, 14%, and 6%, respectively (Fig. 1b).  
306  $C_xH_yO_z$  dominates contributing 74% of the annual median mixing ratios of total  
307 organics, followed by  $C_xH_y$ ,  $C_xH_yO_zN_i$ , and  $C_xH_yN_i$ , with proportions of 22%, 2%,  
308 and 2%, respectively (Fig. 1c). In addition to these resolved formulae, we also  
309 detect 18 peaks containing other elements such as S, Cl, Si, etc., and 79  
310 CH(O)(N) peaks that do not comply with nitrogen rules, which we consider as  
311 fragments or free radicals. Others are unknown peaks for which formulae  
312 cannot be assigned or water clusters/fragments excluded from analysis. The  
313 mixing ratios of organic vapors vary substantially in urban Beijing, ranging from  
314 0.01 parts per trillion (ppt) to 10 parts per billion (ppb) in volume under a time  
315 resolution of 1 min, with many species detected at sub-ppt levels notably (Fig.  
316 1d). The units of the mixing ratio in the following text are all volume fractions.  
317 As the molecular masses of organics increase, their annual median mixing  
318 ratios decrease. The mixing ratios of  $C_xH_yO_z$  and  $C_xH_yO_zN_i$  categories start to  
319 decrease below the ppt level above molecular weights of 160 and 125,  
320 respectively.

321 With enhanced sensitivity and mass resolution, an increased number of  
322 formulae have been identified compared to traditional PTR-MS measurements  
323 in urban Beijing, especially formulae with lower mixing ratios and higher oxygen  
324 contents. Note that most organics with low mixing ratios have high oxygen  
325 content. 44% number of formulae measured in this study are at sub-ppt level  
326 while 31% number of formulae are between 1 and 10 ppt (Fig. 1e). Only  
327 compounds detected above ppt levels were previously reported in urban sites  
328 within Beijing (Sheng et al., 2018; Li et al., 2019), as well as at a suburban site  
329 located 100 km southwest of Beijing (He et al., 2022). Simultaneously, organic  
330 vapors with multiple oxygens ( $C_xH_yO_{\geq 3}$  and  $C_xH_yO_{\geq 3}N_i$  species) have been  
331 successfully detected in this study in the urban atmosphere. Traditionally, they  
332 have been often recognized as total  $C_xH_yO_{\geq 3}$  species, with no individual  
333 analysis in traditional PTR-MS (Yuan et al., 2023; Li et al., 2022b; He et al.,  
334 2022). Many other studies only focus on reporting OVOCs containing up to 2-3  
335 oxygens or omit to address the presence of nitrogen containing OVOCs (Wang  
336 et al., 2021a; Liu et al., 2022). The low mixing ratios and high wall losses of  
337 organic vapors with multiple oxygens impact the detection in traditional PTR-  
338 MS (Breitenlechner et al., 2017). Figure 2a reinterprets the mass defect plot of  
339 measured organics with a focus on oxygen numbers, ranging from 0 to 8. The

340 analysis of mixing ratio levels and variations of organic vapors with multiple  
341 oxygens ( $\geq 3$ ) are shown in [Section 3.2](#). Organic vapors with low oxygen content  
342 ( $\leq 2$ ) are reported in [Section 3.3](#). Subsequent comparison of Vocus-PTR and  
343 traditional PTR in urban Beijing and both Vocus-PTR measurements in urban  
344 Beijing and European forests are also shown in [Section 3.3](#).

### 345 **3.2 Organic vapors with high oxygen content**

346 195 observed organics with multiple oxygen atoms account for 38% in number  
347 of the total organics, including 136 species of  $C_xH_yO_{\geq 3}$  and 59 species of  
348  $C_xH_yO_{\geq 3}N_i$ . Organics with oxygen numbers 3 and 4 dominates within the  
349  $C_xH_yO_{\geq 3}$  and  $C_xH_yO_{\geq 3}N_i$  species ([Fig. 2b](#) and [Fig. 2c](#)). Organics with oxygen  
350 number of 3, 4, 5, and  $\geq 6$  comprise 15%, 11%, 7%, and 6% of the total species  
351 number of  $C_xH_yO_z$  compounds, respectively. While compounds with oxygen  
352 number of 3, 4, 5, and  $\geq 6$  comprise 15%, 12%, 7%, and 2% of the total species  
353 number of  $C_xH_yO_zN_i$  compounds, respectively.

354 The measured organic vapors with multiple oxygens are mainly intermediate  
355 volatile organic compounds (IVOCs) and semi-volatile organic compounds  
356 (SVOCs). The dominant carbon numbers range from 5 to 9 and DBE between  
357 1-5, accounting for over three-quarters of the total species number of organic  
358 vapors with multiple oxygens ([Fig. 3a](#) and [Fig. 3b](#)). The maximum occurrence  
359 of organic vapors with 3 or 4 oxygen atoms is observed within the carbon range  
360 of 7-8 and a DBE value of 2. For organic species with 5 or more oxygens, they  
361 reach their peak at a smaller carbon number of 4-5 and a higher DBE value of  
362 3. Aromatic VOCs have DBE values no smaller than 4, while aliphatic VOCs  
363 usually have DBE values smaller than 2. For organic vapors with DBE between  
364 2-3, they are likely oxidation products of aliphatic and aromatic VOCs (Wang et  
365 al., 2021b; Nie et al., 2022). For the same number of carbon atoms, organic  
366 vapors with a higher number of oxygen atoms exhibit a higher carbon oxidation  
367 state (as shown in [Figure S5](#)). Compared to organic vapors with 3 or 4 oxygen  
368 atoms, organic vapors with 5 or more oxygens have undergone more extensive  
369 atmospheric oxidation and functionalization processes (Kroll et al., 2011;  
370 Isaacman-Vanwertz et al., 2018). Based on calculated volatility, 81% of the  
371 species are IVOCs, and the remaining 19% are SVOCs ([Fig. 3c](#)). With the  
372 increase in oxygen number, the volatility of the compounds gradually decreases,  
373 while the potential partitioning to aerosols increases, manifested by a gradual  
374 reduction in the peak values of the  $\log_{10}C_0$ . Compounds containing nitrogen,  
375 referred to shaded bars with white stripes in [Figure 3c](#), have a lower volatility  
376 compared to non-nitrogen species.

377 The annual median mixing ratio of measured organic vapors with multiple  
378 oxygens in median  $\pm$  standard deviation is 2.0 ppb  $\pm$  0.9 ppb, accounting for 4%  
379 of the total  $C_xH_yO_z$  and  $C_xH_yO_zN_i$  mixing ratios. For  $C_xH_yO_z$  category, the annual  
380 median mixing ratios of species with 3, 4, 5, and  $\geq 6$  oxygens are 1.4 ppb, 186.0

381 ppt, 17.8 ppt, and 5.9 ppt, respectively. For  $C_xH_yO_zN_i$  category, the annual  
382 median mixing ratios of species with 3, 4, 5, and  $\geq 6$  oxygens are 49.6, 24.5, 2.4,  
383 and 0.5 ppt, respectively (Fig. 2d and 2e). Organic vapors with 3 oxygens  
384 constitute the overwhelming majority of the mixing ratio of measured organic  
385 vapors with more than three oxygens. As a result, the mixing ratio-weighted  
386 carbon number and DBE distributions (Fig. 3d and Fig. 3e) are significantly  
387 different from that of species number distributions for organic vapors with  
388 multiple oxygens. The mixing ratios of species with carbon numbers ranging  
389 from 2 to 6 are significantly higher, with those containing four carbons exhibiting  
390 the highest mixing ratios. Similarly, the mixing ratios of species with DBE  
391 ranging from 0-4 are notably higher than that of other DBE values. As  
392 compounds containing 3 oxygens dominate the mixing ratio, IVOCs nearly  
393 entirely contribute to the mixing ratio-weighted volatility of organic vapors with  
394 multiple oxygens (Fig. 3f). The mixing ratios of organic vapors with multiple  
395 oxygens measured in this study are higher than other studies, which will be  
396 detailed in Section 3.3.

397 Though the contribution of the measured IVOCs and SVOCs to the overall VOC  
398 mixing ratio is low, their contribution to the condensational growth rates is non-  
399 negligible, which may influence the growth of new particles (Ehn et al., 2014),  
400 SOA formation (Jimenez et al., 2009), and haze (Nie et al., 2022). The  
401 condensational growth rates of total organic vapors are calculated, including  
402 extremely low, low, and semi volatile organic compounds detected by nitrate-  
403 CIMS and I/SVOCs detected by Vocus-PTR. The contribution to the  
404 condensational growth rate from I/SVOCs detected by Vocus-PTR increases  
405 with particle size and decreases with temperature. For 8 nm particles, the  
406 contribution of SVOCs detected by Vocus-PTR is 9%, while IVOCs contribute  
407 1%. For 40 nm particles, the contribution of SVOCs increases to 13%, and  
408 IVOCs rise to 4%. At sub-zero temperatures for 8 nm particles, the SVOC  
409 contribution detected by Vocus-PTR can reach up to 21%, with IVOCs  
410 contributing 10%.

411 The molecular formulae of the measured organic vapors with multiple oxygens  
412 are displayed in the mass spectra, categorized by carbon numbers ranging from  
413 2-11 (Fig. 4 and Table S4). Many of the formulae are reported as oxidation  
414 products of various VOC precursors in previous studies. Take isoprene as an  
415 example, detected formulae are reported as various oxidation products of  
416 isoprene, including  $C_5H_{10}O_3$  and subsequent oxidation products in C5 species,  
417 e.g.,  $C_5H_8O_6$ ,  $C_5H_9NO_4$ , etc. (Wennberg et al., 2018). For several C4 species,  
418 such as  $C_4H_7NO_4$ ,  $C_4H_4O_3$ , etc., they are reported as oxidation products of two  
419 additional important oxidation products of isoprene, methacrolein (MACR) and  
420 methyl vinyl ketone (MVK). We also see formulae reported as oxidation  
421 products of precursors such as benzene (C6) (Priestley et al., 2021), alkyl-  
422 substituted benzenes (C7-C9) (Pan and Wang, 2014; Wang et al., 2020c;

423 Cheng et al., 2021), and monoterpenes (C<sub>10</sub>) (Rolletter et al., 2019). Besides,  
424 we can also detect some organic vapors with relatively low DBE ( $\leq 3$ ), which  
425 may originate from the oxidation of aliphatic precursors. For example, C<sub>5</sub>H<sub>8</sub>O<sub>4</sub>  
426 observed are reported as one of the oxidation products of C<sub>5</sub> aldehyde, the  
427 photolysis of which release OH radicals. This mechanism may explain the  
428 source gap of OH radicals between simulations and observations in low  
429 nitrogen oxide and high VOCs regimes (Yang et al., 2024). Note that these  
430 species may be oxidation products as reported by previous studies; however,  
431 confirming this would require additional techniques such as GC.

432 Measured molecular formulae may react with OH radicals, contributing to OH  
433 reactivity. The calculated OH reactivity of organic vapors with multiple oxygens  
434 account for 6% of the total detected VOCs, with an average annual value of 1.2  
435 s<sup>-1</sup>. Previous studies show differences between measured and calculated or  
436 modeled OH reactivity (Hansen et al., 2014), and unmeasured species from  
437 photochemical oxidation likely explain this gap (Ferracci et al., 2018). Therefore,  
438 the OH reactivity contributed by detected organic vapors with multiple oxygens  
439 in this study may potentially reduce this gap, thereby improve the accuracy of  
440 diagnosis of sensitivity regimes for ozone formation (Wang et al., 2024). Using  
441 Vocus-PTR has the potential to simultaneously measure both precursors and  
442 multi-generational oxygenated products, which is beneficial for studying the  
443 evolution process of organic compounds in the atmosphere.

444 As for the seasonal variations, the overall mixing ratio of organic vapors with  
445 multiple oxygens is the highest in winter, followed by summer, spring and the  
446 lowest in autumn (Fig. 5a). The mixing ratios expressed in median  $\pm$  standard  
447 deviation (ppb  $\pm$  ppb) are 1.9  $\pm$  0.5, 1.9  $\pm$  0.9, 1.4  $\pm$  1.2, and 2.2  $\pm$  0.8 for spring,  
448 summer, autumn, and winter, respectively. Compounds with different oxygens  
449 exhibit different seasonal variations, shown in Figure 5b and 5c and Table S5.  
450 For C<sub>x</sub>H<sub>y</sub>O<sub>z</sub> with 3 or 4 oxygens, the mixing ratios are higher in winter than in  
451 other seasons, while for compounds containing 5 or more oxygens, the mixing  
452 ratios are highest in summer. For C<sub>x</sub>H<sub>y</sub>O<sub>z</sub>N<sub>i</sub> with 3 or 4 oxygens, the mixing  
453 ratios are high in both summer and winter, while for compounds containing 5 or  
454 more oxygens, the mixing ratios are high in summer and spring. As the oxygen  
455 number increases, the contribution from secondary sources becomes greater,  
456 and the high mixing ratio of oxidants in summer intensifies this process. Thus,  
457 the fraction of the mixing ratio of compounds with multiple oxygens increases  
458 with the oxygen number in summer (Fig. 5d). In winter, the mixing ratios of  
459 compounds containing five or more oxygens are substantially suppressed,  
460 which may be due to reduced generation. Alternatively, it could be that these  
461 compounds belong to SVOCs, with a majority being partitioned onto particulate  
462 matter at low temperatures.

463 The seasonal variations of organic vapors with multiple oxygens differ from  
464 those of total OVOCs (Fig. S6), with the latter's mixing ratio being primarily

465 influenced by organic vapors containing 1-2 oxygen atoms. The mixing ratio of  
466 total OVOCs in winter is substantially higher than in the other three seasons,  
467 followed by autumn and summer, with the lowest mixing ratio observed in spring.  
468 The seasonal variations of OVOCs are partly caused by the variation of mixing  
469 layer height (Li et al., 2023), which is lowest in winter. Cluster analysis is  
470 performed to further explore the dominated driving factors of the seasonal  
471 variations of organic vapors with multiple oxygens. Three clusters are identified  
472 in each season based on the diurnal profiles of each compound. To increase  
473 the interpretability of the clusters, two of them are merged. [Figure 6](#) and [Figure](#)  
474 [S7](#) shows the cluster results for organic vapors with multiple oxygens. For  
475 comparison, cluster analysis is performed on organic vapors with 1-2 oxygens  
476 as well ([Fig. S8](#) and [Fig. S9](#)).

477 Daytime clusters, where the peak occurs during the daytime, were identified  
478 across the four seasons for organic vapors with multiple oxygens (shown as  
479 cluster 1 in [Fig. 6](#)). Daytime clusters start to rise at 6:00-7:00 (6:00 for summer  
480 and 7:00 for other seasons), peak at 11:00-14:00 and then slowly decrease,  
481 following the diurnal variation of solar radiation (Li et al., 2023), ozone and  
482 temperature ([Fig. S2](#)). [Figure S10](#) further demonstrates the dependence of  
483 daytime clusters on temperature. The mixing ratio of daytime clusters show an  
484 apparent increase in summer (when temperature is higher than 15 °C), which  
485 indicates that higher temperatures accompanied by an increase in solar  
486 radiation and ozone favors the formation of daytime clusters. The number and  
487 corresponding mixing ratios of species allocated to the daytime clusters vary in  
488 four seasons. In summer, the vast majority of species (76%) exhibit daytime  
489 characteristics, with a mixing ratio percentage as high as 82%, which may be  
490 related to the strongest solar radiation (Li et al., 2023) and lowest NO<sub>x</sub>  
491 concentrations ([Fig. S2](#)). The contribution of daytime clusters in autumn is also  
492 significant, with 68% and 61% of the species and mixing ratios being accounted  
493 for. The noon peaks of daytime clusters in winter and spring are relatively less  
494 pronounced, with the species and mixing ratio day/night ratios also being  
495 comparatively lower. The afternoon peak of daytime clusters in autumn and  
496 winter are accompanied by a decrease in mixing layer height (Li et al., 2023).  
497 For organic vapors with 1 or 2 oxygens, a significant daytime cluster was  
498 observed only in summer ([Fig. S8 d-f](#)).

499 Another cluster type is considered to be nighttime clusters, as the  
500 corresponding species have their highest mixing ratios at night. Unlike the  
501 daytime cluster, the diurnal variations of nighttime clusters are different in four  
502 seasons ([Fig. 6](#)). In spring, the nighttime cluster comprises over 87% of species  
503 and 75% of mixing ratios, and it peaks at 4:00 with low daytime values. The  
504 nighttime clusters in winter and autumn show bimodal diurnal variations, with  
505 the highest peak occurring during the night from 19:00 to 23:00, and the second  
506 peak appearing during the day from 8:00 to 12:00. 45% and 32% of species

507 exhibit the characteristics of the nighttime cluster in winter and autumn,  
508 constituting 59% and 39% of the mixing ratio, respectively. The contribution of  
509 the nighttime cluster is minimal in summer, reaching its peak at midnight. We  
510 found that each nighttime cluster of organic vapors with multiple oxygens shows  
511 good consistency with the corresponding major clusters of organic vapors  
512 containing 1-2 oxygens (Fig. S8 and Fig. S11), while the mixing ratios during  
513 midday differ. Nighttime clusters also show better consistency with PM<sub>2.5</sub>  
514 compared to daytime clusters (Fig. S2), which may be related to mixed sources.

515 Most organic vapors with multiple oxygens could be assigned to different  
516 clusters in different seasons (Fig. S12). Only a small number of species can be  
517 categorized into the same cluster in four seasons. Figure S13 shows the  
518 average C, H, O, and N number of species assigned to daytime cluster 0-4  
519 times during the four seasons. As compounds exhibit more characteristics  
520 associated with daytime cluster, there is no significant change in the carbon  
521 number, but there is an increase in hydrogen and oxygen number, and a  
522 decrease in nitrogen number. This may be due to multi-step oxidation reactions  
523 in the atmosphere, causing an increase in oxygen number and DBE of species  
524 (Kroll et al., 2011; Isaacman-Vanwertz et al., 2018), with diurnal variations  
525 peaking at noon as a result of the strongest photochemistry. The decreasing  
526 trend of the number of nitrogen atoms in Figure S13 indicates that nitrogen  
527 containing compounds measured in this study are more likely to come from  
528 nocturnal production or emissions. Regarding the average elemental  
529 composition (C, H, O, and N) of species assigned to two clusters (see Fig. S14),  
530 daytime clusters typically exhibit higher oxygen content and lower H/C  
531 compared to nighttime clusters, providing further evidence supporting the  
532 atmospheric photochemical origin of daytime clusters. The nighttime clusters  
533 have higher nitrogen contents than daytime clusters, indicating more of the  
534 impacts of nocturnal sources.

### 535 **3.3 Organic vapors with low oxygen content**

536 In addition to multiple oxygens, organic vapors with low oxygen content were  
537 also measured in urban Beijing in this study. Here we primarily discuss  
538 comparisons between the results of this study and those of previous studies.  
539 The mixing ratios and variations of typical VOCs measured in this study are  
540 comparable to the results obtained by traditional PTR-MS measurements in  
541 both urban Beijing and neighboring regions. Figure S15 shows the diurnal  
542 profiles of 12 representative VOCs in four seasons. OVOCs of C<sub>2</sub>H<sub>4</sub>O, C<sub>3</sub>H<sub>6</sub>O,  
543 and C<sub>4</sub>H<sub>4</sub>O, usually identified as acetaldehyde, acetone, and furan, are mainly  
544 from anthropogenic sources as reported by previous studies (Qian et al., 2019).  
545 Their diurnal variations exhibit a characteristic of being higher at night and lower  
546 during the day, similar to other studies reported in Beijing during the winter  
547 (Sheng et al., 2018; He et al., 2022). The mixing ratios of acetaldehyde, methyl

548 ethyl ketone (MEK), and furan in winter are slightly lower than those observed  
549 in winter Beijing in 2016 and 2018 (Sheng et al., 2018; He et al., 2022). The  
550 winter mixing ratios of acetone are higher than other seasons and observed in  
551 other studies, indicating an unknown emission source during winter. The mixing  
552 ratios of benzene (C<sub>6</sub>H<sub>6</sub>), toluene (C<sub>7</sub>H<sub>8</sub>), and naphthalene (C<sub>10</sub>H<sub>8</sub>) in winter are  
553 slightly lower than reported in winter in Beijing during the past few years (Sheng  
554 et al., 2018; Li et al., 2019; He et al., 2022), possibly due to improvements in  
555 air pollution policies, especially those targeting emissions from residential  
556 combustion and motor vehicles (Liu et al., 2023). As for phenols, the mixing  
557 ratios of C<sub>6</sub>H<sub>6</sub>O are similar to measurement at a background site in the North  
558 China Plain in winter, while the mixing ratios of C<sub>7</sub>H<sub>8</sub>O are much lower than that  
559 (He et al., 2022). High mixing ratios of biogenic emissions in summer are  
560 observed, for example isoprene (C<sub>5</sub>H<sub>8</sub>) and the sum of its oxidation products  
561 MACR and MVK (Apel et al., 2002) have peak mixing ratios of 2.6 ppb and 0.6  
562 ppb, respectively. Their mixing ratios in winter are lower and consistent with  
563 other studies (Sheng et al., 2018; He et al., 2022).

564 The mixing ratio fractions of organic categories in urban Beijing using Vocus-  
565 PTR differ from the results obtained using traditional PTR-MS. Previous studies  
566 in Beijing have only reported a few selected VOCs up to around 100 species,  
567 resulting in limited results on systematic characterizations of VOCs using PTR-  
568 MS in Beijing (Sheng et al., 2018; Li et al., 2019; Wang et al., 2021a; Liu et al.,  
569 2022). Therefore, we compare with a suburban site, Gucheng, which is located  
570 100 km southwest from our site. The two sites (urban Beijing and Gucheng) are  
571 both located in the North China Plain and are subject to regional air pollutions  
572 simultaneously. [Figure S16](#) shows the comparison results of five categories,  
573 including C<sub>x</sub>H<sub>y</sub>, C<sub>x</sub>H<sub>y</sub>O, C<sub>x</sub>H<sub>y</sub>O<sub>2</sub>, C<sub>x</sub>H<sub>y</sub>O<sub>≥3</sub>, and N/S containing compounds. The  
574 first difference is that the mixing ratio fraction of species containing two or more  
575 oxygens measured by Vocus-PTR is higher than those measured by traditional  
576 PTR-MS. The mixing ratio fractions of C<sub>x</sub>H<sub>y</sub>O<sub>2</sub> and C<sub>x</sub>H<sub>y</sub>O<sub>≥3</sub> in Vocus-PTR are  
577 12% and 4%, respectively, whereas they are 6% and 1% for traditional PTR-  
578 MS. In terms of mixing ratios, the mixing ratio of C<sub>x</sub>H<sub>y</sub>O<sub>≥3</sub> is approximately  
579 double in Vocus-PTR compared to traditional PTR-MS, while the mixing ratio of  
580 C<sub>x</sub>H<sub>y</sub>O is half compared to traditional PTR-MS measurement. The mixing ratio  
581 of C<sub>x</sub>H<sub>y</sub>O<sub>2</sub> remains similar. This is because Vocus-PTR can detect more OVOCs  
582 with multiple oxygens due to its high sensitivity and mass resolution, whereas  
583 due to its low transmission efficiency for low masses, it is difficult to detect high  
584 mixing ratio OVOCs such as methanol and formaldehyde. The other difference  
585 is that the mixing ratio and the corresponding fraction of C<sub>x</sub>H<sub>y</sub> species measured  
586 by Vocus-PTR are much lower than those measured by traditional PTR. For  
587 several major C<sub>x</sub>H<sub>y</sub> compounds such as benzene, C7, C8, and C9 aromatics,  
588 their mixing ratios are comparable between the two methods. The main  
589 difference between the two methods lies in the mixing ratio of low-mass  
590 hydrocarbons. Overall, when applied to the urban atmosphere, Vocus-PTR has

591 advantages in measuring oxygenated VOCs, especially with multiple oxygens.  
592 However, it has limitations in measuring low molecular weight VOCs due to the  
593 low-mass cutoff in the transmission efficiency.

594 The molecular characteristics of organic vapors measured by Vocus-PTR in  
595 urban Beijing show several differences from those in forested areas (Li et al.,  
596 2020; Huang et al., 2021; Li et al., 2021). Firstly, organics up to 300 m/z can be  
597 observed in forested areas, while organics up to 230 m/z are observed (Fig.  
598 1a). Two main reasons are responsible for this. The complexity of the species  
599 introduces challenges in interpreting mass spectra, which is evidenced by the  
600 total number of species being similar to existing atmospheric measurements  
601 using Vocus-PTR, despite a narrower mass range in this study. The higher  
602 particulate matter concentrations in urban areas provide a larger sink for  
603 organic vapors (Deng et al., 2020), and this loss effect is especially pronounced  
604 for compounds with high molecular weights due to their lower volatility. The  
605 second difference is that,  $C_xH_yO_z$  and  $C_xH_yO_zN_i$  species are the dominant  
606 organics in both urban and forested areas, whilst  $C_xH_yN_i$  species are more  
607 common and abundant in urban areas, which may come from biomass burning  
608 emissions (Laskin et al., 2009). Thirdly, VOCs with low carbon and oxygen  
609 number play a more significant role in total organic mixing ratio compared to  
610 results from forested regions. As shown in Figure S17a,  $C_2$  and  $C_3$  organics  
611 contribute 79% of the total organic mixing ratio in this study, while  $C_4$ - $C_6$   
612 organics contribute approximately 75% in forested regions. In contrast to  
613 forested areas, where VOCs and IVOCs mixing ratios are comparable, the  
614 majority of the total organic mixing ratio is attributed to VOCs in this study (Fig.  
615 S17b). Typical  $C_2$  and  $C_3$  organics, such as  $C_3H_6O$ ,  $C_2H_4O$ , and  $C_2H_4O_2$ ,  
616 contribute 14%, 11%, and 5%, respectively, to the total organic mixing ratio,  
617 which are mainly originated from anthropogenic emissions including industrial  
618 and vehicular activities, solvent utilization, and other sources (Qian et al., 2019).

## 619 **4 Conclusions**

620 In this study, we explore the molecular and seasonal characteristics of organic  
621 vapors in urban Beijing using a Vocus-PTR over four seasons. A total of 895  
622 peaks are observed, and 512 of them can be assigned to formulae. The  
623 contribution of  $C_xH_yO_z$  species is most significant, which compose up to 54% of  
624 the number and 74% of the mixing ratios of total organics. With enhanced  
625 sensitivity and mass resolution, an increased number of species were observed  
626 compared to traditional PTR-MS measurements in urban Beijing, especially  
627 compounds with lower mixing ratios and higher oxygen content. 44% species  
628 in number measured in this study are at sub-ppt level and 38% species in  
629 number contain 3-8 oxygens, resulting in a higher fraction of species containing  
630 three or more oxygens compared to traditional PTR-MS measurements.



631 Organic vapors with low oxygen content are comparable to those obtained in  
632 both urban Beijing and neighboring regions, and they exert a more substantial  
633 influence on the overall organic mixing in forested areas.

634 The mixing ratio of organic vapors with multiple oxygens accounts for 4% of the  
635 total VOC mixing ratio, with the highest levels observed in winter, followed by  
636 summer, spring, and the lowest in autumn. These vapors also make a non-  
637 negligible contribution to condensational growth and OH reactivity. In summer,  
638 the majority of species are aligned to daytime cluster (peaking at noon),  
639 primarily originating from the photooxidation process. As the oxygen number  
640 increases, the impact of the photooxidation process becomes more  
641 pronounced, leading to an increase in both mixing ratio and proportion of  
642 organic vapors with multiple oxygens during summer. In spring and winter when  
643 the nighttime cluster (peaking at night) dominated, the variations of organic  
644 vapors with multiple oxygens are strongly correlated with organic vapors with  
645 one or two oxygens. The measured compositions and seasonal variabilities of  
646 organic vapors with multiple oxygens emphasize the importance of high  
647 sensitivity and high mass resolution measurements in urban atmosphere,  
648 suggesting prospective for future research.

#### 649 **Data availability**

650 Data are available upon request from the corresponding author.

#### 651 **Supporting Information**

652 The content of the SI includes the map of the observation site (Fig. S1); the  
653 diurnal variations of PM<sub>2.5</sub>, O<sub>3</sub>, NO<sub>x</sub>, RH, and T in four seasons (Fig. S2);  
654 calibration results of mixed calibration gases (Fig. S3); average limits of  
655 detection (1 min) for detected compounds (Fig. S4); carbon oxidation state of  
656 organic vapors with different oxygens (Fig. S5); boxplot of total OVOC mixing  
657 ratios in four seasons (Fig. S6); diurnal variation cluster results of organic  
658 vapors with multiple oxygens (Fig. S7); cluster results of organic vapors with  
659 one or two oxygens (Fig. S8-S9); dependence of daytime clusters on  
660 temperature (Fig. S10); dependence of nighttime clusters on major clusters of  
661 organic vapors with 1-2 oxygens (Fig. S11); the distribution of organic vapors  
662 with multiple oxygens across different clusters (Fig. S12); average C, H, O, and  
663 N number of organic vapors containing multiple oxygens with different diurnal  
664 patterns (Fig. S13); average C, H, O, and N number of organic vapors  
665 containing multiple oxygens in two clusters (Fig. S14); diurnal profiles of  
666 representative VOCs in four seasons (Fig. S15); comparison results with  
667 Gucheng site (Fig. S16); molecular characteristics of total measured organic  
668 vapors by Vocus-PTR (Fig. S17); the observation periods of Vocus-PTR (Table

669 S1); information about calibration gases (Table S2); corrected fragments and  
670 water clusters (Table S3); main  $C_xH_yO_{\geq 3}$  and  $C_xH_yO_{\geq 3}N$  species measured in  
671 this study (Table S4), and seasonal mixing ratios of OVOCs with multiple  
672 oxygens (Table S5).

### 673 **Author contributions**

674 Conceptualization: JJ and ZA. Data collection and analysis: ZA, RY, XZ, XxL,  
675 YY, JG, YuL, YZ, and XuL. Writing-original draft: ZA. Writing-review and editing:  
676 XxL, DL, YaL, DW, CY, KH, DRW, FNK, and JJ.

### 677 **Competing interests**

678 At least one of the (co-)authors is a member of the editorial board of  
679 *Atmospheric Chemistry and Physics*.

### 680 **Financial support**

681 This work has been supported by the National Natural Science Foundation of  
682 China (Grant NO. 22206097, 22188102, and 22106083) and Samsung PM<sub>2.5</sub>  
683 SRP.

### 684 **References**

685 Apel, E. C., Riemer, D. D., Hills, A., Baugh, W., Orlando, J., Faloon, I., Tan, D.,  
686 Brune, W., Lamb, B., Westberg, H., Carroll, M. A., Thornberry, T., and Geron,  
687 C. D.: Measurement and interpretation of isoprene fluxes and isoprene,  
688 methacrolein, and methyl vinyl ketone mixing ratios at the PROPHET site  
689 during the 1998 Intensive, *J. Geophys. Res.: Atmos.*, 107,  
690 10.1029/2000jd000225, 2002.

691 Bianchi, F., Kurten, T., Riva, M., Mohr, C., Rissanen, M. P., Roldin, P., Berndt,  
692 T., Crouse, J. D., Wennberg, P. O., Mentel, T. F., Wildt, J., Junninen, H.,  
693 Jokinen, T., Kulmala, M., Worsnop, D. R., Thornton, J. A., Donahue, N.,  
694 Kjaergaard, H. G., and Ehn, M.: Highly Oxygenated Organic Molecules (HOM)  
695 from Gas-Phase Autoxidation Involving Peroxy Radicals: A Key Contributor to  
696 Atmospheric Aerosol, *Chem. Rev.*, 119, 3472-3509,  
697 10.1021/acs.chemrev.8b00395, 2019.

698 Breitenlechner, M., Fischer, L., Hainer, M., Heinritzi, M., Curtius, J., and Hansel,  
699 A.: PTR3: An Instrument for Studying the Lifecycle of Reactive Organic Carbon  
700 in the Atmosphere, *Anal Chem.*, 89, 5824-5831,  
701 10.1021/acs.analchem.6b05110, 2017.

702 Cai, R. and Jiang, J.: A new balance formula to estimate new particle formation  
703 rate: reevaluating the effect of coagulation scavenging, *Atmos. Chem. Phys.*,  
704 17, 12659-12675, 10.5194/acp-17-12659-2017, 2017.

705 Cappellin, L., Karl, T., Probst, M., Ismailova, O., Winkler, P. M., Soukoulis, C.,

- 706 Aprea, E., Mark, T. D., Gasperi, F., and Biasioli, F.: On quantitative  
707 determination of volatile organic compound concentrations using proton  
708 transfer reaction time-of-flight mass spectrometry, *Environ Sci Technol*, 46,  
709 2283-2290, 10.1021/es203985t, 2012.
- 710 Carter, W. P. L.: Development of Ozone Reactivity Scales for Volatile Organic  
711 Compounds, *Air & Waste*, 44, 881-899, 10.1080/1073161X.1994.10467290,  
712 1994.
- 713 Chang, Y., Wang, H., Gao, Y., Jing, S., Lu, Y., Lou, S., Kuang, Y., Cheng, K.,  
714 Ling, Q., Zhu, L., Tan, W., and Huang, R. J.: Nonagricultural emissions  
715 dominate urban atmospheric amines as revealed by mobile measurements,  
716 *Geophys. Res. Lett.*, 10.1029/2021gl097640, 2022.
- 717 Cheng, X., Chen, Q., Jie Li, Y., Zheng, Y., Liao, K., and Huang, G.: Highly  
718 oxygenated organic molecules produced by the oxidation of benzene and  
719 toluene in a wide range of OH exposure and NO<sub>x</sub> conditions, *Atmos. Chem.*  
720 *Phys.*, 21, 12005-12019, 10.5194/acp-21-12005-2021, 2021.
- 721 Coggon, M. M., Stockwell, C. E., Clafin, M. S., Pfannerstill, E. Y., Xu, L., Gilman,  
722 J. B., Marcantonio, J., Cao, C., Bates, K., Gkatzelis, G. I., Lamplugh, A., Katz,  
723 E. F., Arata, C., Apel, E. C., Hornbrook, R. S., Piel, F., Majluf, F., Blake, D. R.,  
724 Wisthaler, A., Canagaratna, M., Lerner, B. M., Goldstein, A. H., Mak, J. E., and  
725 Warneke, C.: Identifying and correcting interferences to PTR-ToF-MS  
726 measurements of isoprene and other urban volatile organic compounds, *Atmos.*  
727 *Meas. Tech.*, 17, 801-825, 10.5194/amt-17-801-2024, 2024.
- 728 de Gouw, J. and Warneke, C.: Measurements of volatile organic compounds in  
729 the earth's atmosphere using proton-transfer-reaction mass spectrometry,  
730 *Mass Spectrom Rev*, 26, 223-257, 10.1002/mas.20119, 2007.
- 731 Deng, C., Fu, Y., Dada, L., Yan, C., Cai, R., Yang, D., Zhou, Y., Yin, R., Lu, Y.,  
732 Li, X., Qiao, X., Fan, X., Nie, W., Kontkanen, J., Kangasluoma, J., Chu, B., Ding,  
733 A., Kerminen, V. M., Paasonen, P., Worsnop, D. R., Bianchi, F., Liu, Y., Zheng,  
734 J., Wang, L., Kulmala, M., and Jiang, J.: Seasonal Characteristics of New  
735 Particle Formation and Growth in Urban Beijing, *Environ Sci Technol*, 54, 8547-  
736 8557, 10.1021/acs.est.0c00808, 2020.
- 737 Ehn, M., Thornton, J. A., Kleist, E., Sipilä, M., Junninen, H., Pullinen, I., Springer,  
738 M., Rubach, F., Tillmann, R., Lee, B., Lopez-Hilfiker, F., Andres, S., Acir, I.-H.,  
739 Rissanen, M., Jokinen, T., Schobesberger, S., Kangasluoma, J., Kontkanen, J.,  
740 Nieminen, T., Kurtén, T., Nielsen, L. B., Jørgensen, S., Kjaergaard, H. G.,  
741 Canagaratna, M., Maso, M. D., Berndt, T., Petäjä, T., Wahner, A., Kerminen, V.-  
742 M., Kulmala, M., Worsnop, D. R., Wildt, J., and Mentel, T. F.: A large source of  
743 low-volatility secondary organic aerosol, *Nature*, 506, 476-479,  
744 10.1038/nature13032, 2014.
- 745 Ferracci, V., Heimann, I., Abraham, N. L., Pyle, J. A., and Archibald, A. T.: Global  
746 modelling of the total OH reactivity: investigations on the "missing" OH sink and  
747 its atmospheric implications, *Atmos. Chem. Phys.*, 18, 7109-7129,  
748 10.5194/acp-18-7109-2018, 2018.
- 749 Fischer, L., Breitenlechner, M., Canaval, E., Scholz, W., Striednig, M., Graus,  
750 M., Karl, T. G., Petäjä, T., Kulmala, M., and Hansel, A.: First eddy covariance  
751 flux measurements of semi-volatile organic compounds with the PTR3-TOF-  
752 MS, *Atmos. Meas. Tech.*, 14, 8019-8039, 10.5194/amt-14-8019-2021, 2021.
- 753 Gentner, D. R., Worton, D. R., Isaacman, G., Davis, L. C., Dallmann, T. R.,  
754 Wood, E. C., Herndon, S. C., Goldstein, A. H., and Harley, R. A.: Chemical  
755 Composition of Gas-Phase Organic Carbon Emissions from Motor Vehicles and  
756 Implications for Ozone Production, *Environ. Sci. Technol.*, 47, 11837-11848,

- 757 10.1021/es401470e, 2013.
- 758 Gilman, J. B., Lerner, B. M., Kuster, W. C., Goldan, P. D., Warneke, C., Veres,  
759 P. R., Roberts, J. M., de Gouw, J. A., Burling, I. R., and Yokelson, R. J.: Biomass  
760 burning emissions and potential air quality impacts of volatile organic  
761 compounds and other trace gases from fuels common in the US, *Atmos. Chem.*  
762 *Phys.*, 15, 13915-13938, 10.5194/acp-15-13915-2015, 2015.
- 763 Goldstein, A. H. and Galbally, I. E.: Known and Unexplored Organic  
764 Constituents in the Earth's Atmosphere, *Environ. Sci. Technol.*, 41, 1514-1521,  
765 10.1021/es072476p, 2007.
- 766 Gueneron, M., Erickson, M. H., VanderSchelden, G. S., and Jobson, B. T.: PTR-  
767 MS fragmentation patterns of gasoline hydrocarbons, *Int. J. Mass Spectrom.*,  
768 379, 97-109, 10.1016/j.ijms.2015.01.001, 2015.
- 769 Hallquist, M., Wenger, J. C., Baltensperger, U., Rudich, Y., Simpson, D., Claeys,  
770 M., Dommen, J., Donahue, N. M., George, C., Goldstein, A. H., Hamilton, J. F.,  
771 Herrmann, H., Hoffmann, T., Iinuma, Y., Jang, M., Jenkin, M. E., Jimenez, J. L.,  
772 Kiendler-Scharr, A., Maenhaut, W., McFiggans, G., Mentel, T. F., Monod, A.,  
773 Prévôt, A. S. H., Seinfeld, J. H., Surratt, J. D., Szmigielski, R., and Wildt, J.: The  
774 formation, properties and impact of secondary organic aerosol: current and  
775 emerging issues, *Atmos. Chem. Phys.*, 9, 5155-5236, 10.5194/acp-9-5155-  
776 2009, 2009.
- 777 Hansel, A., Jordan, A., Holzinger, R., Prazeller, P., Vogel, W., and Lindinger, W.:  
778 Proton transfer reaction mass spectrometry: on-line trace gas analysis at the  
779 ppb level, *International Journal of Mass Spectrometry and Ion Processes*, 149-  
780 150, 609-619, [https://doi.org/10.1016/0168-1176\(95\)04294-U](https://doi.org/10.1016/0168-1176(95)04294-U), 1995.
- 781 Hansen, R. F., Griffith, S. M., Dusanter, S., Rickly, P. S., Stevens, P. S., Bertman,  
782 S. B., Carroll, M. A., Erickson, M. H., Flynn, J. H., Grossberg, N., Jobson, B. T.,  
783 Lefer, B. L., and Wallace, H. W.: Measurements of total hydroxyl radical  
784 reactivity during CABINEX 2009 &ndash; Part 1: field measurements, *Atmos.*  
785 *Chem. Phys.*, 14, 2923-2937, 10.5194/acp-14-2923-2014, 2014.
- 786 He, X., Yuan, B., Wu, C., Wang, S., Wang, C., Huangfu, Y., Qi, J., Ma, N., Xu,  
787 W., Wang, M., Chen, W., Su, H., Cheng, Y., and Shao, M.: Volatile organic  
788 compounds in wintertime North China Plain: Insights from measurements of  
789 proton transfer reaction time-of-flight mass spectrometer (PTR-ToF-MS),  
790 *Journal of Environmental Sciences*, 10.1016/j.jes.2021.08.010, 2022.
- 791 Huang, W., Li, H., Sarnela, N., Heikkinen, L., Tham, Y. J., Mikkilä, J., Thomas,  
792 S. J., Donahue, N. M., Kulmala, M., and Bianchi, F.: Measurement report:  
793 Molecular composition and volatility of gaseous organic compounds in a boreal  
794 forest – from volatile organic compounds to highly oxygenated organic  
795 molecules, *Atmos. Chem. Phys.*, 21, 8961-8977, 10.5194/acp-21-8961-2021,  
796 2021.
- 797 Isaacman-VanWertz, G., Massoli, P., O'Brien, R., Lim, C., Franklin, J. P., Moss,  
798 J. A., Hunter, J. F., Nowak, J. B., Canagaratna, M. R., Misztal, P. K., Arata, C.,  
799 Roscioli, J. R., Herndon, S. T., Onasch, T. B., Lambe, A. T., Jayne, J. T., Su, L.,  
800 Knopf, D. A., Goldstein, A. H., Worsnop, D. R., and Kroll, J. H.: Chemical  
801 evolution of atmospheric organic carbon over multiple generations of oxidation,  
802 *Nat Chem*, 10, 462-468, 10.1038/s41557-018-0002-2, 2018.
- 803 Jahn, L. G., Tang, M., Blomdahl, D., Bhattacharyya, N., Abue, P., Novoselac, A.,  
804 Ruiz, L. H., and Misztal, P. K.: Volatile organic compound (VOC) emissions from  
805 the usage of benzalkonium chloride and other disinfectants based on  
806 quaternary ammonium compounds, *Environmental Science: Atmospheres*, 3,  
807 363-373, 10.1039/d2ea00054g, 2023.

808 Jensen, A. R., Koss, A. R., Hales, R. B., and de Gouw, J. A.: Measurements of  
809 volatile organic compounds in ambient air by gas-chromatography and real-  
810 time Vocus PTR-TOF-MS: calibrations, instrument background corrections, and  
811 introducing a PTR Data Toolkit, *Atmos. Meas. Tech.*, 16, 5261-5285,  
812 10.5194/amt-16-5261-2023, 2023.

813 Jimenez, J. L., Canagaratna, M. R., Donahue, N. M., Prevot, A. S. H., Zhang,  
814 Q., Kroll, J. H., DeCarlo, P. F., Allan, J. D., Coe, H., Ng, N. L., Aiken, A. C.,  
815 Docherty, K. S., Ulbrich, I. M., Grieshop, A. P., Robinson, A. L., Duplissy, J.,  
816 Smith, J. D., Wilson, K. R., Lanz, V. A., Hueglin, C., Sun, Y. L., Tian, J.,  
817 Laaksonen, A., Raatikainen, T., Rautiainen, J., Vaattovaara, P., Ehn, M.,  
818 Kulmala, M., Tomlinson, J. M., Collins, D. R., Cubison, M. J., Dunlea, E. J.,  
819 Huffman, J. A., Onasch, T. B., Alfarra, M. R., Williams, P. I., Bower, K., Kondo,  
820 Y., Schneider, J., Drewnick, F., Borrmann, S., Weimer, S., Demerjian, K.,  
821 Salcedo, D., Cottrell, L., Griffin, R., Takami, A., Miyoshi, T., Hatakeyama, S.,  
822 Shimono, A., Sun, J. Y., Zhang, Y. M., Dzepina, K., Kimmel, J. R., Sueper, D.,  
823 Jayne, J. T., Herndon, S. C., Trimborn, A. M., Williams, L. R., Wood, E. C.,  
824 Middlebrook, A. M., Kolb, C. E., Baltensperger, U., and Worsnop, D. R.:  
825 Evolution of Organic Aerosols in the Atmosphere, *Science*, 326, 1525-1529,  
826 10.1126/science.1180353, 2009.

827 Krechmer, J., Lopez-Hilfiker, F., Koss, A., Hutterli, M., Stoermer, C., Deming, B.,  
828 Kimmel, J., Warneke, C., Holzinger, R., Jayne, J., Worsnop, D., Fuhrer, K.,  
829 Gonin, M., and de Gouw, J.: Evaluation of a New Reagent-Ion Source and  
830 Focusing Ion-Molecule Reactor for Use in Proton-Transfer-Reaction Mass  
831 Spectrometry, *Anal Chem*, 90, 12011-12018, 10.1021/acs.analchem.8b02641,  
832 2018.

833 Kroll, J. H., Donahue, N. M., Jimenez, J. L., Kessler, S. H., Canagaratna, M. R.,  
834 Wilson, K. R., Altieri, K. E., Mazzoleni, L. R., Wozniak, A. S., Bluhm, H., Mysak,  
835 E. R., Smith, J. D., Kolb, C. E., and Worsnop, D. R.: Carbon oxidation state as  
836 a metric for describing the chemistry of atmospheric organic aerosol, *Nature*  
837 *Chemistry*, 3, 133-139, 10.1038/nchem.948, 2011.

838 Laskin, A., Smith, J. S., and Laskin, J.: Molecular Characterization of Nitrogen-  
839 Containing Organic Compounds in Biomass Burning Aerosols Using High-  
840 Resolution Mass Spectrometry, *Environ. Sci. Technol.*, 43, 3764-3771,  
841 10.1021/es803456n, 2009.

842 Lewis, A. C., Carslaw, N., Marriott, P. J., Kinghorn, R. M., Morrison, P., Lee, A.  
843 L., Bartle, K. D., and Pilling, M. J.: A larger pool of ozone-forming carbon  
844 compounds in urban atmospheres, *Nature*, 405, 778-781, 2000.

845 Li, H., Almeida, T. G., Luo, Y., Zhao, J., Palm, B. B., Daub, C. D., Huang, W.,  
846 Mohr, C., Krechmer, J. E., Kurtén, T., and Ehn, M.: Fragmentation inside proton-  
847 transfer-reaction-based mass spectrometers limits the detection of ROOR and  
848 ROOH peroxides, *Atmos. Meas. Tech.*, 15, 1811-1827, 10.5194/amt-15-1811-  
849 2022, 2022a.

850 Li, H., Riva, M., Rantala, P., Heikkinen, L., Daellenbach, K., Krechmer, J. E.,  
851 Flaud, P.-M., Worsnop, D., Kulmala, M., Villenave, E., Perraudin, E., Ehn, M.,  
852 and Bianchi, F.: Terpenes and their oxidation products in the French Landes  
853 forest: insights from Vocus PTR-TOF measurements, *Atmos. Chem. Phys.*, 20,  
854 1941-1959, 10.5194/acp-20-1941-2020, 2020.

855 Li, H., Canagaratna, M. R., Riva, M., Rantala, P., Zhang, Y., Thomas, S.,  
856 Heikkinen, L., Flaud, P.-M., Villenave, E., Perraudin, E., Worsnop, D., Kulmala,  
857 M., Ehn, M., and Bianchi, F.: Atmospheric organic vapors in two European pine  
858 forests measured by a Vocus PTR-TOF: insights into monoterpene and  
859 sesquiterpene oxidation processes, *Atmos. Chem. Phys.*, 21, 4123-4147,

860 10.5194/acp-21-4123-2021, 2021.

861 Li, K., Li, J., Tong, S., Wang, W., Huang, R.-J., and Ge, M.: Characteristics of  
862 wintertime VOCs in suburban and urban Beijing: concentrations, emission  
863 ratios, and festival effects, *Atmos. Chem. Phys.*, 19, 8021-8036, 10.5194/acp-  
864 19-8021-2019, 2019.

865 Li, K., Zhang, J., Bell, D. M., Wang, T., Lamkaddam, H., Cui, T., Qi, L., Surdu,  
866 M., Wang, D., Du, L., El Haddad, I., Slowik, J. G., and Prevot, A. S. H.:  
867 Uncovering the dominant contribution of intermediate volatility compounds in  
868 secondary organic aerosol formation from biomass-burning emissions, *Natl Sci  
869 Rev*, 11, nwae014, 10.1093/nsr/nwae014, 2024a.

870 Li, X., Chen, Y., Li, Y., Cai, R., Li, Y., Deng, C., Wu, J., Yan, C., Cheng, H., Liu,  
871 Y., Kulmala, M., Hao, J., Smith, J. N., and Jiang, J.: Seasonal variations in  
872 composition and sources of atmospheric ultrafine particles in urban Beijing  
873 based on near-continuous measurements, *Atmos. Chem. Phys.*, 23, 14801-  
874 14812, 10.5194/acp-23-14801-2023, 2023.

875 Li, X.-B., Yuan, B., Wang, S., Wang, C., Lan, J., Liu, Z., Song, Y., He, X.,  
876 Huangfu, Y., Pei, C., Cheng, P., Yang, S., Qi, J., Wu, C., Huang, S., You, Y.,  
877 Chang, M., Zheng, H., Yang, W., Wang, X., and Shao, M.: Variations and  
878 sources of volatile organic compounds (VOCs) in urban region: insights from  
879 measurements on a tall tower, *Atmos. Chem. Phys.*, 22, 10567-10587,  
880 10.5194/acp-22-10567-2022, 2022b.

881 Li, Y., Cai, R., Yin, R., Li, X., Yuan, Y., An, Z., Guo, J., Stolzenburg, D., Kulmala,  
882 M., and Jiang, J.: A kinetic partitioning method for simulating the condensation  
883 mass flux of organic vapors in a wide volatility range, *J. Aerosol Sci.*, 180,  
884 10.1016/j.jaerosci.2024.106400, 2024b.

885 Liu, Q., Sheng, J., Wu, Y., Ma, Z., Sun, J., Tian, P., Zhao, D., Li, X., Hu, K., Li,  
886 S., Shen, X., Zhang, Y., He, H., Huang, M., Ding, D., and Liu, D.: Source  
887 characterization of volatile organic compounds in urban Beijing and its links to  
888 secondary organic aerosol formation, *Sci. Total Environ.*,  
889 10.1016/j.scitotenv.2022.160469, 2022.

890 Liu, Y., Yin, S., Zhang, S., Ma, W., Zhang, X., Qiu, P., Li, C., Wang, G., Hou, D.,  
891 Zhang, X., An, J., Sun, Y., Li, J., Zhang, Z., Chen, J., Tian, H., Liu, X., and Liu,  
892 L.: Drivers and impacts of decreasing concentrations of atmospheric volatile  
893 organic compounds (VOCs) in Beijing during 2016-2020, *Sci Total Environ*, 906,  
894 167847, 10.1016/j.scitotenv.2023.167847, 2023.

895 Millet, D. B., Baasandorj, M., Farmer, D. K., Thornton, J. A., Baumann, K.,  
896 Brophy, P., Chaliyakunnel, S., de Gouw, J. A., Graus, M., Hu, L., Koss, A., Lee,  
897 B. H., Lopez-Hilfiker, F. D., Neuman, J. A., Paulot, F., Peischl, J., Pollack, I. B.,  
898 Ryerson, T. B., Warneke, C., Williams, B. J., and Xu, J.: A large and ubiquitous  
899 source of atmospheric formic acid, *Atmos. Chem. Phys.*, 15, 6283-6304,  
900 10.5194/acp-15-6283-2015, 2015.

901 Nie, W., Yan, C., Huang, D. D., Wang, Z., Liu, Y., Qiao, X., Guo, Y., Tian, L.,  
902 Zheng, P., Xu, Z., Li, Y., Xu, Z., Qi, X., Sun, P., Wang, J., Zheng, F., Li, X., Yin,  
903 R., Dallenbach, K. R., Bianchi, F., Petäjä, T., Zhang, Y., Wang, M., Schervish,  
904 M., Wang, S., Qiao, L., Wang, Q., Zhou, M., Wang, H., Yu, C., Yao, D., Guo, H.,  
905 Ye, P., Lee, S., Li, Y. J., Liu, Y., Chi, X., Kerminen, V.-M., Ehn, M., Donahue, N.  
906 M., Wang, T., Huang, C., Kulmala, M., Worsnop, D., Jiang, J., and Ding, A.:  
907 Secondary organic aerosol formed by condensing anthropogenic vapours over  
908 China's megacities, *Nature Geoscience*, 15, 255-261, 10.1038/s41561-022-  
909 00922-5, 2022.

910 Noziere, B., Kalberer, M., Claeys, M., Allan, J., D'Anna, B., Decesari, S., Finessi,

- 911 E., Glasius, M., Grgic, I., Hamilton, J. F., Hoffmann, T., Iinuma, Y., Jaoui, M.,  
912 Kahnt, A., Kampf, C. J., Kourtchev, I., Maenhaut, W., Marsden, N., Saarikoski,  
913 S., Schnelle-Kreis, J., Surratt, J. D., Szidat, S., Szmigielski, R., and Wisthaler,  
914 A.: The molecular identification of organic compounds in the atmosphere: state  
915 of the art and challenges, *Chemical Reviews*, 115, 3919-3983,  
916 10.1021/cr5003485, 2015.
- 917 Pan, S. and Wang, L.: Atmospheric oxidation mechanism of m-xylene initiated  
918 by OH radical, *J Phys Chem A*, 118, 10778-10787, 10.1021/jp506815v, 2014.
- 919 Pfannerstill, E. Y., Arata, C., Zhu, Q., Schulze, B. C., Woods, R., Seinfeld, J. H.,  
920 Bucholtz, A., Cohen, R. C., and Goldstein, A. H.: Volatile organic compound  
921 fluxes in the agricultural San Joaquin Valley – spatial distribution, source  
922 attribution, and inventory comparison, *Atmos. Chem. Phys.*, 23, 12753-12780,  
923 10.5194/acp-23-12753-2023, 2023a.
- 924 Pfannerstill, E. Y., Arata, C., Zhu, Q., Schulze, B. C., Ward, R., Woods, R.,  
925 Harkins, C., Schwantes, R. H., Seinfeld, J. H., Bucholtz, A., Cohen, R. C., and  
926 Goldstein, A. H.: Temperature-dependent emissions dominate aerosol and  
927 ozone formation in Los Angeles, *Science*, 384, 1324-1329,  
928 doi:10.1126/science.adg8204, 2024.
- 929 Pfannerstill, E. Y., Arata, C., Zhu, Q., Schulze, B. C., Woods, R., Harkins, C.,  
930 Schwantes, R. H., McDonald, B. C., Seinfeld, J. H., Bucholtz, A., Cohen, R. C.,  
931 and Goldstein, A. H.: Comparison between Spatially Resolved Airborne Flux  
932 Measurements and Emission Inventories of Volatile Organic Compounds in Los  
933 Angeles, *Environ Sci Technol*, 57, 15533-15545, 10.1021/acs.est.3c03162,  
934 2023b.
- 935 Pospisilova, V., Lopez-Hilfiker, F. D., Bell, D. M., El Haddad, I., Mohr, C., Huang,  
936 W., Heikkinen, L., Xiao, M., Dommen, J., Prevot, A. S. H., Baltensperger, U.,  
937 and Slowik, J. G.: On the fate of oxygenated organic molecules in atmospheric  
938 aerosol particles, *Science Advances*, 6, eaax8922, doi:10.1126/sciadv.aax8922,  
939 2020.
- 940 Priestley, M., Bannan, T. J., Le Breton, M., Worrall, S. D., Kang, S., Pullinen, I.,  
941 Schmitt, S., Tillmann, R., Kleist, E., Zhao, D., Wildt, J., Garmash, O., Mehra, A.,  
942 Bacak, A., Shallcross, D. E., Kiendler-Scharr, A., Hallquist, Å. M., Ehn, M., Coe,  
943 H., Percival, C. J., Hallquist, M., Mentel, T. F., and McFiggans, G.: Chemical  
944 characterisation of benzene oxidation products under high- and low-NO<sub>x</sub>  
945 conditions using chemical ionisation mass spectrometry, *Atmos. Chem. Phys.*,  
946 21, 3473-3490, 10.5194/acp-21-3473-2021, 2021.
- 947 Pugliese, G., Ingrisch, J., Meredith, L. K., Pfannerstill, E. Y., Klupfel, T., Meeran,  
948 K., Byron, J., Purser, G., Gil-Loaiza, J., van Haren, J., Dontsova, K.,  
949 Kreuzwieser, J., Ladd, S. N., Werner, C., and Williams, J.: Effects of drought  
950 and recovery on soil volatile organic compound fluxes in an experimental  
951 rainforest, *Nat Commun*, 14, 5064, 10.1038/s41467-023-40661-8, 2023.
- 952 Qian, X., Shen, H., and Chen, Z.: Characterizing summer and winter carbonyl  
953 compounds in Beijing atmosphere, *Atmos. Environ.*, 214,  
954 10.1016/j.atmosenv.2019.116845, 2019.
- 955 Qiao, X., Zhang, Q., Wang, D., Hao, J., and Jiang, J.: Improving data reliability:  
956 A quality control practice for low-cost PM(2.5) sensor network, *Sci Total Environ*,  
957 779, 146381, 10.1016/j.scitotenv.2021.146381, 2021.
- 958 Reinecke, T., Leiminger, M., Jordan, A., Wisthaler, A., and Muller, M.: Ultrahigh  
959 Sensitivity PTR-MS Instrument with a Well-Defined Ion Chemistry, *Anal Chem*,  
960 95, 11879-11884, 10.1021/acs.analchem.3c02669, 2023.

961 Riva, M., Rantala, P., Krechmer, J. E., Peräkylä, O., Zhang, Y., Heikkinen, L.,  
962 Garmash, O., Yan, C., Kulmala, M., Worsnop, D., and Ehn, M.: Evaluating the  
963 performance of five different chemical ionization techniques for detecting  
964 gaseous oxygenated organic species, *Atmos. Meas. Tech.*, 12, 2403-2421,  
965 10.5194/amt-12-2403-2019, 2019.

966 Rolletter, M., Kaminski, M., Acir, I.-H., Bohn, B., Dorn, H.-P., Li, X., Lutz, A.,  
967 Nehr, S., Rohrer, F., Tillmann, R., Wegener, R., Hofzumahaus, A., Kiendler-  
968 Scharr, A., Wahner, A., and Fuchs, H.: Investigation of the  $\alpha$ -pinene  
969 photooxidation by OH in the atmospheric simulation chamber SAPHIR, *Atmos.*  
970 *Chem. Phys.*, 19, 11635-11649, 10.5194/acp-19-11635-2019, 2019.

971 Sekimoto, K., Li, S.-M., Yuan, B., Koss, A., Coggon, M., Warneke, C., and de  
972 Gouw, J.: Calculation of the sensitivity of proton-transfer-reaction mass  
973 spectrometry (PTR-MS) for organic trace gases using molecular properties, *Int.*  
974 *J. Mass Spectrom.*, 421, 71-94, 10.1016/j.ijms.2017.04.006, 2017.

975 Sheng, J., Zhao, D., Ding, D., Li, X., Huang, M., Gao, Y., Quan, J., and Zhang,  
976 Q.: Characterizing the level, photochemical reactivity, emission, and source  
977 contribution of the volatile organic compounds based on PTR-TOF-MS during  
978 winter haze period in Beijing, China, *Atmospheric Research*, 212, 54-63,  
979 10.1016/j.atmosres.2018.05.005, 2018.

980 Sreeram, A., Blomdahl, D., Misztal, P., and Bhasin, A.: High resolution chemical  
981 fingerprinting and real-time oxidation dynamics of asphalt binders using Vocus  
982 Proton Transfer Reaction (PTR-TOF) mass spectrometry, *Fuel*, 320,  
983 10.1016/j.fuel.2022.123840, 2022.

984 Thomas, S. J., Li, H., Praplan, A. P., Hellén, H., and Bianchi, F.: Complexity of  
985 downy birch emissions revealed by Vocus proton transfer reaction time-of-flight  
986 mass spectrometer, *Frontiers in Forests and Global Change*, 5,  
987 10.3389/ffgc.2022.1030348, 2022.

988 Vermeuel, M. P., Novak, G. A., Kilgour, D. B., Claffin, M. S., Lerner, B. M.,  
989 Trowbridge, A. M., Thom, J., Cleary, P. A., Desai, A. R., and Bertram, T. H.:  
990 Observations of biogenic volatile organic compounds over a mixed temperate  
991 forest during the summer to autumn transition, *Atmos. Chem. Phys.*, 23, 4123-  
992 4148, 10.5194/acp-23-4123-2023, 2023.

993 Vettikkat, L., Miettinen, P., Buchholz, A., Rantala, P., Yu, H., Schallhart, S.,  
994 Petäjä, T., Seco, R., Männistö, E., Kulmala, M., Tuittila, E.-S., Guenther, A. B.,  
995 and Schobesberger, S.: High emission rates and strong temperature response  
996 make boreal wetlands a large source of isoprene and terpenes, *Atmos. Chem.*  
997 *Phys.*, 23, 2683-2698, 10.5194/acp-23-2683-2023, 2023.

998 Wang, L., Slowik, J. G., Tong, Y., Duan, J., Gu, Y., Rai, P., Qi, L., Stefenelli, G.,  
999 Baltensperger, U., Huang, R.-J., Cao, J., and Prévôt, A. S. H.: Characteristics  
1000 of wintertime VOCs in urban Beijing: Composition and source apportionment,  
1001 *Atmospheric Environment: X*, 9, 10.1016/j.aeaoa.2020.100100, 2021a.

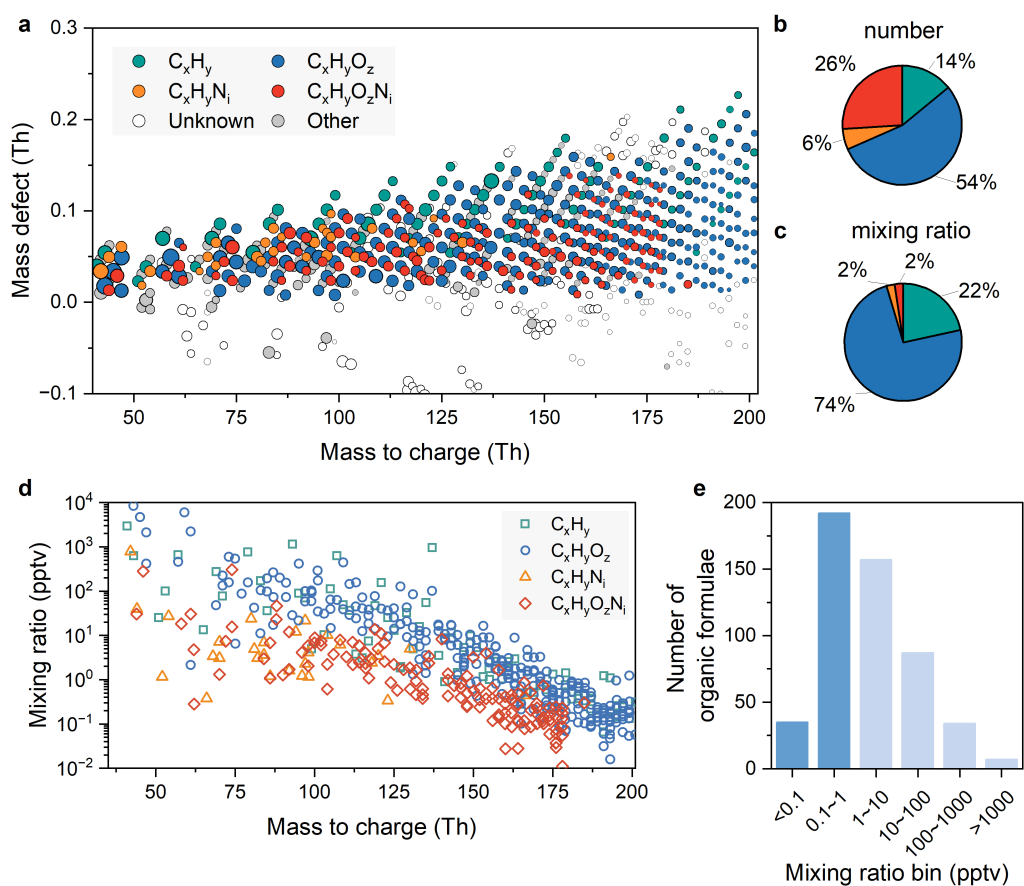
1002 Wang, M., Chen, D., Xiao, M., Ye, Q., Stolzenburg, D., Hofbauer, V., Ye, P.,  
1003 Vogel, A. L., Mauldin, R. L., 3rd, Amorim, A., Baccarini, A., Baumgartner, B.,  
1004 Brilke, S., Dada, L., Dias, A., Duplissy, J., Finkenzeller, H., Garmash, O., He, X.  
1005 C., Hoyle, C. R., Kim, C., Kvashnin, A., Lehtipalo, K., Fischer, L., Molteni, U.,  
1006 Petaja, T., Pospisilova, V., Quelever, L. L. J., Rissanen, M., Simon, M., Tauber,  
1007 C., Tome, A., Wagner, A. C., Weitz, L., Volkamer, R., Winkler, P. M., Kirkby, J.,  
1008 Worsnop, D. R., Kulmala, M., Baltensperger, U., Dommen, J., El-Haddad, I.,  
1009 and Donahue, N. M.: Photo-oxidation of Aromatic Hydrocarbons Produces Low-  
1010 Volatility Organic Compounds, *Environ Sci Technol*, 54, 7911-7921,  
1011 10.1021/acs.est.0c02100, 2020a.



- 1012 Wang, W., Yuan, B., Su, H., Cheng, Y., Qi, J., Wang, S., Song, W., Wang, X.,  
1013 Xue, C., Ma, C., Bao, F., Wang, H., Lou, S., and Shao, M.: A large role of missing  
1014 volatile organic compound reactivity from anthropogenic emissions in ozone  
1015 pollution regulation, *Atmos. Chem. Phys.*, 24, 4017-4027, 10.5194/acp-24-  
1016 4017-2024, 2024.
- 1017 Wang, Y., Yang, G., Lu, Y., Liu, Y., Chen, J., and Wang, L.: Detection of gaseous  
1018 dimethylamine using vocus proton-transfer-reaction time-of-flight mass  
1019 spectrometry, *Atmos. Environ.*, 243, 10.1016/j.atmosenv.2020.117875, 2020b.
- 1020 Wang, Y., Mehra, A., Krechmer, J. E., Yang, G., Hu, X., Lu, Y., Lambe, A.,  
1021 Canagaratna, M., Chen, J., Worsnop, D., Coe, H., and Wang, L.: Oxygenated  
1022 products formed from OH-initiated reactions of trimethylbenzene: autoxidation  
1023 and accretion, *Atmos. Chem. Phys.*, 20, 9563-9579, 10.5194/acp-20-9563-  
1024 2020, 2020c.
- 1025 Wang, Z., Ehn, M., Rissanen, M. P., Garmash, O., Quelever, L., Xing, L.,  
1026 Monge-Palacios, M., Rantala, P., Donahue, N. M., Berndt, T., and Sarathy, S.  
1027 M.: Efficient alkane oxidation under combustion engine and atmospheric  
1028 conditions, *Commun Chem*, 4, 18, 10.1038/s42004-020-00445-3, 2021b.
- 1029 Wennberg, P. O., Bates, K. H., Crouse, J. D., Dodson, L. G., McVay, R. C.,  
1030 Mertens, L. A., Nguyen, T. B., Praske, E., Schwantes, R. H., Smarte, M. D., St  
1031 Clair, J. M., Teng, A. P., Zhang, X., and Seinfeld, J. H.: Gas-Phase Reactions of  
1032 Isoprene and Its Major Oxidation Products, *Chem. Rev.*, 118, 3337-3390,  
1033 10.1021/acs.chemrev.7b00439, 2018.
- 1034 Williams, J. and Koppmann, R.: Volatile Organic Compounds in the Atmosphere:  
1035 An Overview, in: *Volatile Organic Compounds in the Atmosphere*, 1-32,  
1036 <https://doi.org/10.1002/9780470988657.ch1>, 2007.
- 1037 Wohl, C., Güell-Bujons, Q., Castillo, Y. M., Calbet, A., and Simó, R.: Volatile  
1038 Organic Compounds Released by *Oxyrrhis marina* Grazing on *Isochrysis*  
1039 *galbana*, *Oceans*, 4, 151-169, 10.3390/oceans4020011, 2023.
- 1040 Wu, C., Wang, C., Wang, S., Wang, W., Yuan, B., Qi, J., Wang, B., Wang, H.,  
1041 Wang, C., Song, W., Wang, X., Hu, W., Lou, S., Ye, C., Peng, Y., Wang, Z.,  
1042 Huangfu, Y., Xie, Y., Zhu, M., Zheng, J., Wang, X., Jiang, B., Zhang, Z., and  
1043 Shao, M.: Measurement report: Important contributions of oxygenated  
1044 compounds to emissions and chemistry of volatile organic compounds in urban  
1045 air, *Atmos. Chem. Phys.*, 20, 14769-14785, 10.5194/acp-20-14769-2020, 2020.
- 1046 Xu, X., Stee, L. L. P., Williams, J., Beens, J., Adahchour, M., Vreuls, R. J. J.,  
1047 Brinkman, U. A., and Lelieveld, J.: Comprehensive two-dimensional gas  
1048 chromatography (GC × GC) measurements of volatile organic compounds in  
1049 the atmosphere, *Atmospheric Chemistry & Physics*, 3, 665-682, 2003.
- 1050 Yacovitch, T. I., Lerner, B. M., Canagaratna, M. R., Daube, C., Healy, R. M.,  
1051 Wang, J. M., Fortner, E. C., Majluf, F., Claflin, M. S., Roscioli, J. R., Lunny, E.  
1052 M., and Herndon, S. C.: Mobile Laboratory Investigations of Industrial Point  
1053 Source Emissions during the MOOSE Field Campaign, *Atmosphere*, 14,  
1054 10.3390/atmos14111632, 2023.
- 1055 Yang, X., Wang, H., Lu, K., Ma, X., Tan, Z., Long, B., Chen, X., Li, C., Zhai, T.,  
1056 Li, Y., Qu, K., Xia, Y., Zhang, Y., Li, X., Chen, S., Dong, H., Zeng, L., and Zhang,  
1057 Y.: Reactive aldehyde chemistry explains the missing source of hydroxyl  
1058 radicals, *Nat Commun*, 15, 1648, 10.1038/s41467-024-45885-w, 2024.
- 1059 Ye, C., Yuan, B., Lin, Y., Wang, Z., Hu, W., Li, T., Chen, W., Wu, C., Wang, C.,  
1060 Huang, S., Qi, J., Wang, B., Wang, C., Song, W., Wang, X., Zheng, E.,  
1061 Krechmer, J. E., Ye, P., Zhang, Z., Wang, X., Worsnop, D. R., and Shao, M.:

- 1062 Chemical characterization of oxygenated organic compounds in the gas phase  
1063 and particle phase using iodide CIMS with FIGAERO in urban air, *Atmos. Chem.*  
1064 *Phys.*, 21, 8455-8478, 10.5194/acp-21-8455-2021, 2021.
- 1065 Yu, Y., Guo, S., Wang, H., Shen, R., Zhu, W., Tan, R., Song, K., Zhang, Z., Li,  
1066 S., Chen, Y., and Hu, M.: Importance of Semivolatile/Intermediate-Volatility  
1067 Organic Compounds to Secondary Organic Aerosol Formation from Chinese  
1068 Domestic Cooking Emissions, *Environ. Sci. Technol.*,  
1069 10.1021/acs.estlett.2c00207, 2022.
- 1070 Yuan, B., Koss, A. R., Warneke, C., Coggon, M., Sekimoto, K., and de Gouw,  
1071 J. A.: Proton-Transfer-Reaction Mass Spectrometry: Applications in  
1072 Atmospheric Sciences, *Chem. Rev.*, 117, 13187-13229,  
1073 10.1021/acs.chemrev.7b00325, 2017.
- 1074 Yuan, B., Koss, A., Warneke, C., Gilman, J. B., Lerner, B. M., Stark, H., and de  
1075 Gouw, J. A.: A high-resolution time-of-flight chemical ionization mass  
1076 spectrometer utilizing hydronium ions ( $H_3O^+$  ToF-CIMS) for measurements of  
1077 volatile organic compounds in the atmosphere, *Atmos. Meas. Tech.*, 9, 2735-  
1078 2752, 10.5194/amt-9-2735-2016, 2016.
- 1079 Yuan, Q., Zhang, Z., Chen, Y., Hui, L., Wang, M., Xia, M., Zou, Z., Wei, W., Ho,  
1080 K. F., Wang, Z., Lai, S., Zhang, Y., Wang, T., and Lee, S.: Origin and  
1081 transformation of volatile organic compounds at a regional background site in  
1082 Hong Kong: Varied photochemical processes from different source regions, *Sci*  
1083 *Total Environ.*, 168316, 10.1016/j.scitotenv.2023.168316, 2023.
- 1084 Zaytsev, A., Breitenlechner, M., Koss, A. R., Lim, C. Y., Rowe, J. C., Kroll, J. H.,  
1085 and Keutsch, F. N.: Using collision-induced dissociation to constrain sensitivity  
1086 of ammonia chemical ionization mass spectrometry ( $NH_4^+$  CIMS) to  
1087 oxygenated volatile organic compounds, *Atmos Meas Tech*, 12, 1861-1870,  
1088 10.5194/amt-12-1861-2019, 2019a.
- 1089 Zaytsev, A., Koss, A. R., Breitenlechner, M., Krechmer, J. E., Nihill, K. J., Lim,  
1090 C. Y., Rowe, J. C., Cox, J. L., Moss, J., Roscioli, J. R., Canagaratna, M. R.,  
1091 Worsnop, D. R., Kroll, J. H., and Keutsch, F. N.: Mechanistic study of the  
1092 formation of ring-retaining and ring-opening products from the oxidation of  
1093 aromatic compounds under urban atmospheric conditions, *Atmos Chem Phys*,  
1094 19, 15117-15129, 10.5194/acp-19-15117-2019, 2019b.
- 1095 Zhang, Y., Xu, W., Zhou, W., Li, Y., Zhang, Z., Du, A., Qiao, H., Kuang, Y., Liu,  
1096 L., Zhang, Z., He, X., Cheng, X., Pan, X., Fu, Q., Wang, Z., Ye, P., Worsnop, D.  
1097 R., and Sun, Y.: Characterization of organic vapors by a Vocus proton-transfer-  
1098 reaction mass spectrometry at a mountain site in southeastern China, *Sci Total*  
1099 *Environ.*, 919, 170633, 10.1016/j.scitotenv.2024.170633, 2024.
- 1100 Zhao, J. and Zhang, R.: Proton transfer reaction rate constants between  
1101 hydronium ion ( $H_3O^+$ ) and volatile organic compounds, *Atmos. Environ.*, 38,  
1102 2177-2185, 10.1016/j.atmosenv.2004.01.019, 2004.
- 1103  
1104

1105 **Figures**

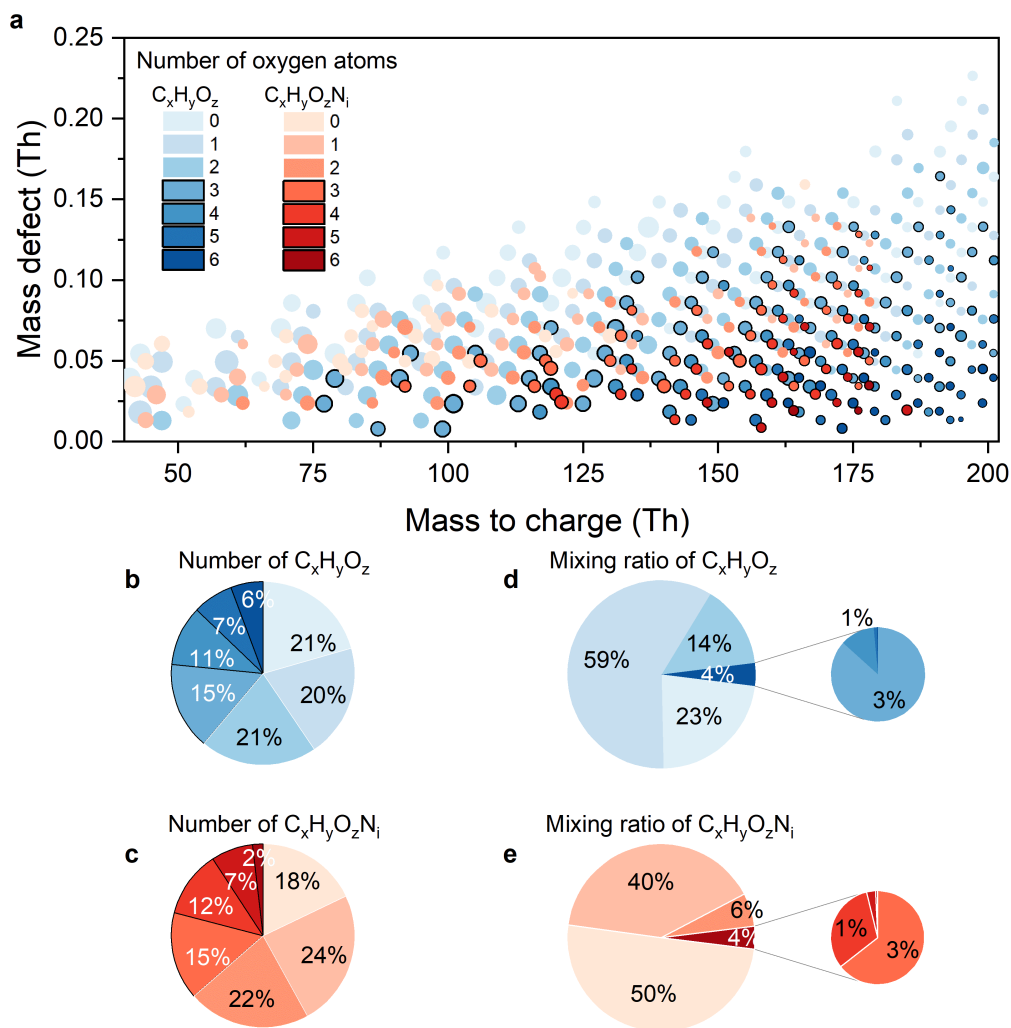


1106

1107 Figure 1. Identified formulae in urban Beijing using Vocus-PTR. (a) Mass defect  
 1108 plot. The sizes of the bubbles represent the annual median mixing ratios. The  
 1109 bubbles are colored by different elemental compositions as labeled in the  
 1110 legend. The “unknown” refers to fitted peaks without matched formula. The  
 1111 “other” refers to peaks containing elements other than C, H, O, and N or  
 1112 fragment peaks (or radicals). (b) Pie chart of the number of identified formulae.  
 1113 (c) Pie chart of the annual median mixing ratios of identified formulae. The color  
 1114 scheme of the pie charts is the same to that of the mass defect plot. (d) The  
 1115 annual median mixing ratios of identified formulae versus their masses. (e)  
 1116 Histogram of annual mixing ratios of identified formulae. Bins with values less  
 1117 than 1 ppt are emphasized in dark blue color.

1118

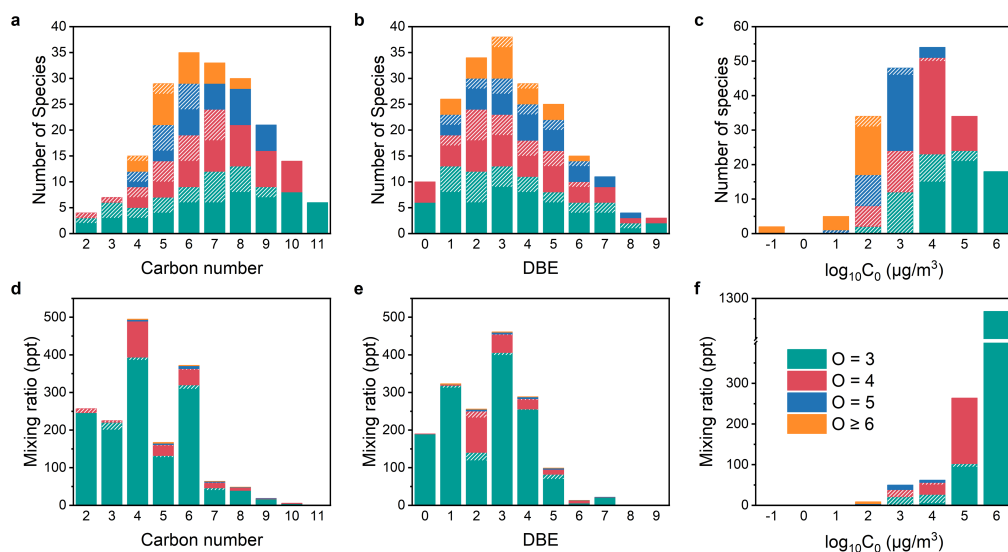
1119



1120

1121 Figure 2. Organic vapors of different oxygen content. (a) Mass defect plot. The  
 1122 sizes of the bubbles represent the annual median mixing ratios. The bubbles  
 1123 are colored by different oxygen numbers as labeled in the legend. Bubbles  
 1124 representing organic vapors with 3 or more oxygens are highlighted with black  
 1125 borders. Bars labeled as 6 refers to organic vapors with oxygen number equal  
 1126 or larger than 6. (b) Pie chart of the number of  $C_xH_yO_z$  species. (c) Pie chart of  
 1127 the number of  $C_xH_yO_zN_i$  species. (d) Pie chart of the mixing ratio of  $C_xH_yO_z$   
 1128 species. (e) Pie chart of the mixing ratio of  $C_xH_yO_zN_i$  species. The color scheme  
 1129 of the pie charts is the same to that of the mass defect plot.

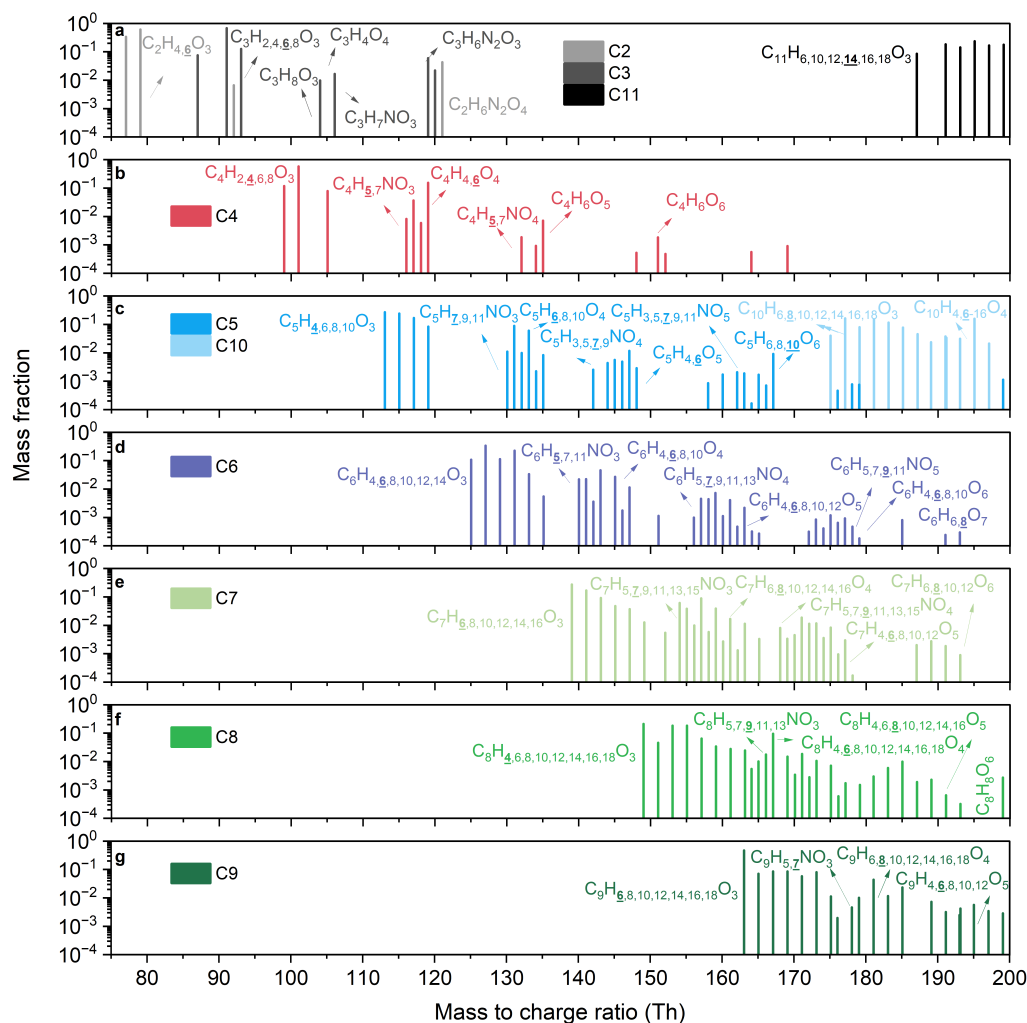
1130



1131

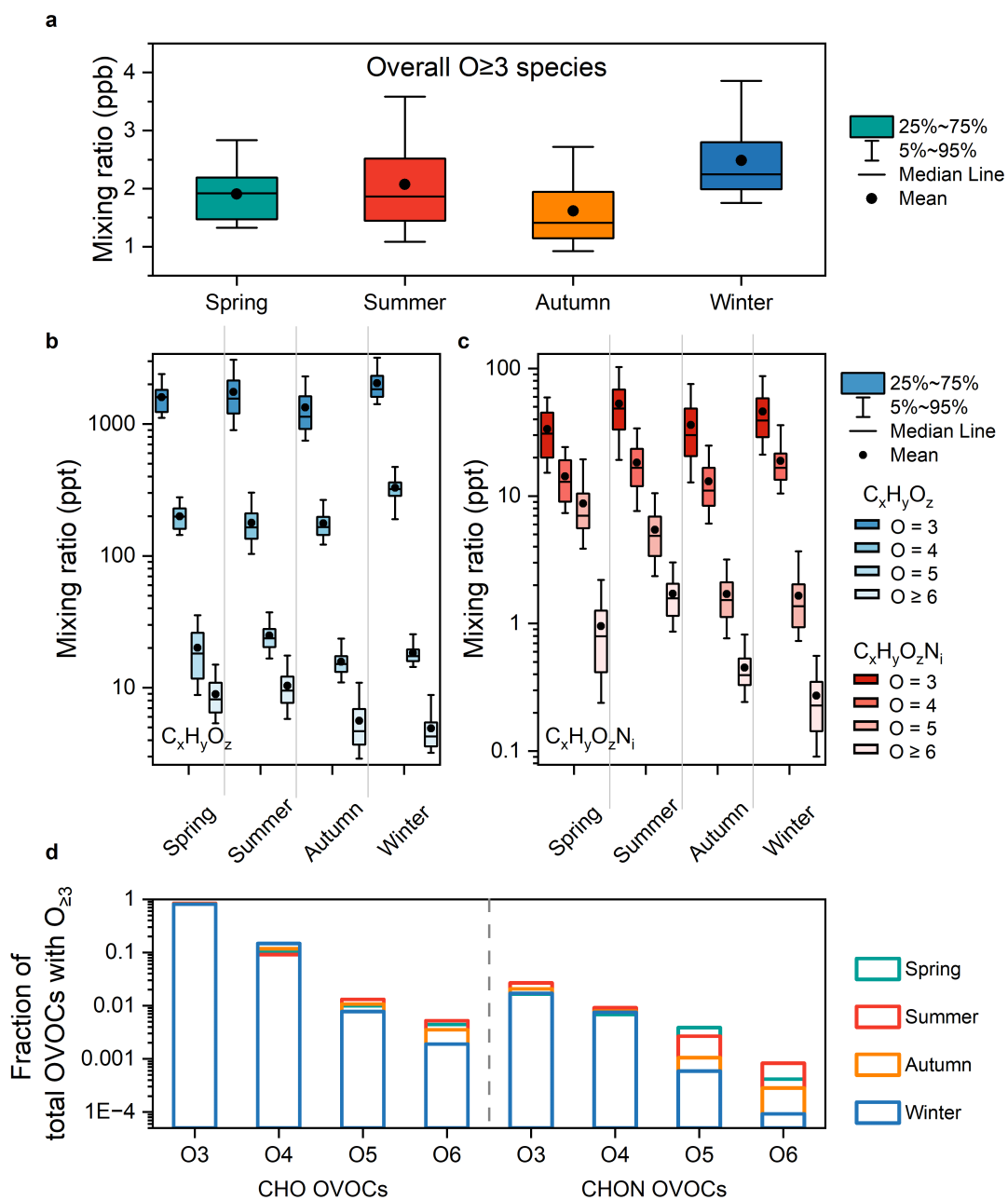
1132 Figure 3. Distribution of carbon number, double bond equivalent (DBE), and  
 1133 volatility of organic vapors with multiple oxygens. Panels (a) - (c) represent  
 1134 species number distributions of carbon number, DBE, and volatility, respectively.  
 1135 Panels (d) - (e) represent mixing ratio distributions of carbon number, DBE, and  
 1136 volatility, respectively. Different color of bars refers to compounds with different  
 1137 oxygen content. Bars without white stripes represent C<sub>x</sub>H<sub>y</sub>O<sub>≥3</sub>, while shaded  
 1138 bars with white stripes represent C<sub>x</sub>H<sub>y</sub>O<sub>≥3</sub>N. Y axes refer to annual median  
 1139 mixing ratios.

1140



1141

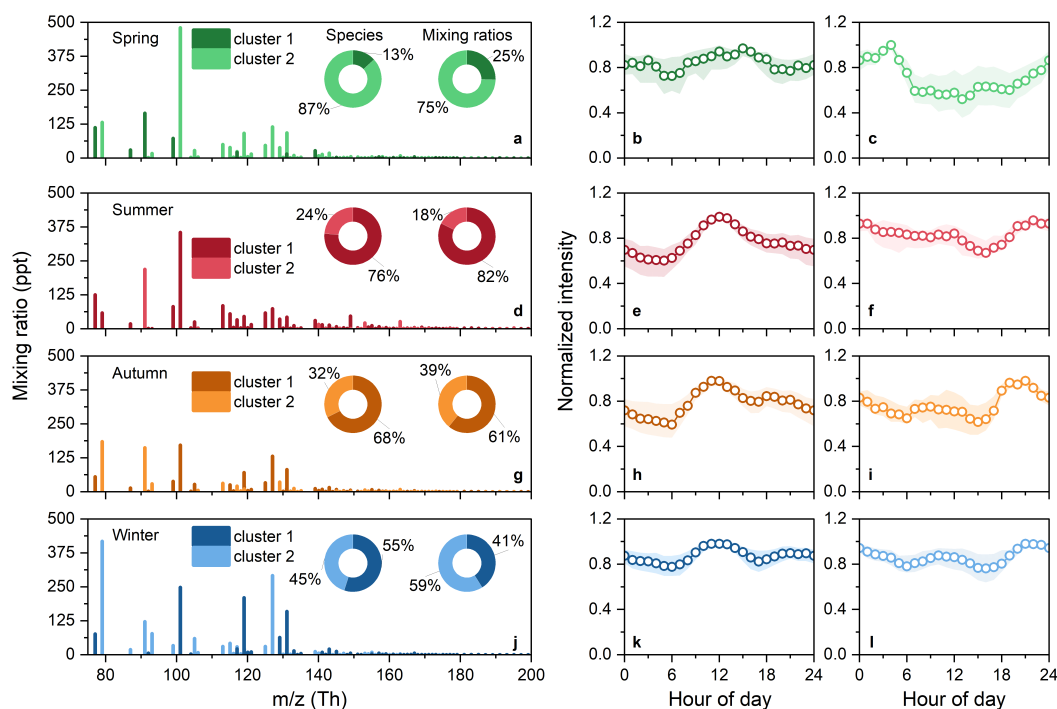
1142 Figure 4. Mass spectra of organic vapors with multiple oxygens with different  
 1143 carbon numbers: (a) C2, C3, and C11; (b) C4; (c) C5 and C10; (d) C6; (e) C7;  
 1144 (f) C8; (g) C9. The y axis shows the annual median mixing ratio fraction of  
 1145 organic vapors for each carbon number, which means that for different organic  
 1146 vapors with the same carbon number, the sum of the mixing ratio fractions  
 1147 equals 1. The unprotonated formulae of organics vapors with multiple oxygens  
 1148 are labelled. In molecular formulas with the same number of carbons and  
 1149 oxygens, the hydrogen content in the organic vapors with the highest intensity  
 1150 is emphasized by bold and underlined formatting.



1151

1152 Figure 5. Seasonal variations of organic vapors with multiple oxygens in urban  
 1153 Beijing. (a) Total organic vapors with multiple oxygens. (b) C<sub>x</sub>H<sub>y</sub>O<sub>z</sub> with different  
 1154 oxygens. (c) C<sub>x</sub>H<sub>y</sub>O<sub>z</sub>N<sub>i</sub> with different oxygens. (d) Fractions of organic vapors  
 1155 with different oxygens of total organic vapors with multiple oxygens.

1156



1157

1158 Figure 6. Cluster results of organic vapors with multiple oxygens in four seasons.  
 1159 (a) – (c) Cluster results for spring. (a) Mass spectra of organic vapors with  
 1160 multiple oxygens in spring. Y axis is the median mixing ratio of each compound.  
 1161 Two different shades of colors are used to distinguish between two clusters.  
 1162 Two pie charts represent the distribution of species numbers and mixing ratios  
 1163 of organic vapors for two clusters. (b) Normalized median diurnal variation of  
 1164 cluster 1, daytime cluster. (c) Normalized median diurnal variation of cluster 2,  
 1165 nighttime cluster. The shaded areas in the graph (b) and (c) represent the 25<sup>th</sup>  
 1166 and 75<sup>th</sup> percentiles. (d) – (f) Cluster results for summer. (g) to (i) Cluster results  
 1167 for autumn. (j) – (l) Cluster results for winter.